UHASSELT
KNOWLEDGE IN ACTION

Faculteit Wetenschappen

master in materiomics

Masterthesis

Development of measurement setups to determine the chiroptical properties of chiral hybrid perovskites

Kevin van Glabbeeck

Scriptie ingediend tot het behalen van de graad van master in materiomics

PROMOTOR :
Prof. dr. Wouter VAN GOMPEL
Prof. dr. ir. Koen VANDEWAL

2023
2024

UHASSELT
KNOWLEDGE IN ACTION

www.uhasselt.be
Universiteit Hasselt
Campus Hasselt:
Martelarenlaan 42 | 3500 Hasselt
Campus Diepenbeek:
Agoralaan Gebouw D | 3590 Diepenbeek

Faculteit Wetenschappen

master in materiomics

Masterthesis

Development of measurement setups to determine the chiroptical properties of chiral hybrid perovskites

Kevin van Glabbeeck

Scriptie ingediend tot het behalen van de graad van master in materiomics

PROMOTOR :

Prof. dr. Wouter VAN GOMPEL

Prof. dr. ir. Koen VANDEWAL

Development of measurement setups to determine the chiroptical properties of chiral hybrid perovskites

Kevin van Glabbeeck[1,2,*], *Melissa Van Landeghem*[2], *Aleksandra Ciesielska*[1],
Wouter Van Gompel[1] *and Koen Vandewal*[2]

[1] Hybrid Materials Design, Institute for Materials Research (IMO), Hasselt University,
Agoralaan 1-Building D, 3590 Diepenbeek, Belgium
[2] Organic Opto-Electronics, Institute for Materials Research (IMO), Hasselt University,
Agoralaan 1-Building D, 3590 Diepenbeek, Belgium
E-mail: kevin.vanglabbeeck@student.uhasselt.be

Keywords: chirality, perovskites, CD spectroscopy, CPL spectroscopy, CP-photodetector

Abstract: Circularly polarized light will become more important in the future thanks to its applications in highly efficient displays, enantiospecific discrimination, and quantum computing. Today, circularly polarized light is made with a linear polarizer and a quarter-wave plate. However, this reduces the light intensity by 50 %. This problem can be overcome by direct emission of circularly polarized light via chiral materials, such as chiral hybrid perovskites. A circular dichroism (CD) and circularly polarized luminescence (CPL) spectrometer are used to determine different chiroptic properties of these materials. In this project, a sensitive CPL setup will be built, which can be converted into a CD spectrometer. Both spectrometers will be validated with reference materials. From the reference chiroptic measurements, it can be noted that care must be taken to identify and circumvent measurement artifacts. After optimization of the CPL setup, dissymmetry factors in the order of 10^{-2} can be obtained. CD measurements still have too many artifacts to obtain accurate results. Therefore, further research and optimization is needed. As a demonstration of an application of chiral materials, photodetectors from chiral hybrid perovskites are constructed. However, further optimization is required to measure these photodetectors accurately.

Abstract in Dutch: Circulair gepolariseerd licht zal in de toekomst belangrijker worden dankzij toepassingen in zeer efficiënte beeldschermen, enantiospecifieke discriminatie en *quantumcomputing*. Tegenwoordig wordt circulair gepolariseerd licht gemaakt met een lineaire polarisator en een *quarter-wave plate*. Dit vermindert de lichtintensiteit echter met 50 %. Dit probleem kan worden opgelost door directe emissie van circulair gepolariseerd licht via chirale materialen, zoals chirale hybride perovskieten. Een circulair dichroïsme (CD) en circulair gepolariseerde luminescentie (CPL) spectrometer zal worden gebruikt om verschillende chiroptische eigenschappen van deze materialen te bepalen. In dit project zal een gevoelige CPL opstelling gebouwd worden, die omgebouwd kan worden tot een CD spectrometer. Beide spectrometers

zullen gevalideerd worden met referentiematerialen. Uit de chiroptische referentiemetingen kan worden afgeleid dat zorg moet worden besteed aan het identificeren en omzeilen van meetartefacten. Na optimalisatie van de CPL opstelling kunnen dissymmetriefactoren in de grootte orde van 10^{-2} worden verkregen. CD metingen hebben nog steeds te veel artefacten om nauwkeurige resultaten te verkrijgen. Daarom is verder onderzoek en optimalisatie nodig. Als demonstratie van een toepassing van chirale materialen zijn fotodetectoren van chirale hybride perovskieten gebouwd. Echter verdere optimalisatie is nodig om deze fotodetectoren nauwkeurig te kunnen meten.

1 Introduction

In the past decade, hybrid organic-inorganic perovskites (HOIPs) have emerged as materials for solar cells, light-emitting diodes (LEDs), and photodetectors. This is due to their excellent properties, such as high absorption coefficients, long charge diffusion lengths, high defect tolerance, and tunable structure.[1] The general formula of a three-dimensional (3D) HOIP is ABX_3 (see **Figure 1** for a schematic view), where A is a (organic) cation (Cs^+, $CH_3NH_3^+$ (MA), or $HC(NH_2)_2^+$ (FA)), B is a divalent metallic cation (Ge^{2+}, Sn^{2+}, or Pb^{2+}), and X is a halide anion (Cl^-, Br^-, or I^-).[2,3] Using larger organic cations will cause lower-dimensional structures to form, which can be thought of as slicing the 3D structure along a specific crystallographic plane to create thin layers. This leads to two-dimensional (2D) or quasi-2D HOIPs, with the former generally having enhanced environmental stability compared to their 3D counterpart.[2,4]

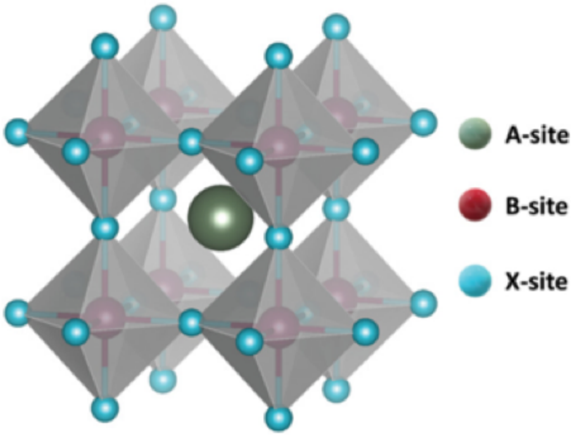

Figure 1. Schematic view of the halide perovskite structure, where the corner-shared $[BX_6]$ octahedrons form a 3D framework with A cations located in the framework cavities.[3]

Further expansion of the applicability of these HOIPs may be achieved through the introduction of chirality. As a result, the chiral HOIP will be imparted with chiroptical properties by implementing chiral organic cations. The first chiral hybrid perovskite (CHP) was synthesized and crystallographically characterized in 2003.[5] However, further research on CHPs was not conducted until 2017. Since then, more strategies have been utilized to functionalize perovskites with chirality and study the chiroptical properties. In particular, the dichroic behavior was characterized through circular dichroism (CD) spectroscopy, which measures the differential absorption of left- and right-handed circularly polarized (CP) light and can be indicated by the absorption dissymmetry factor (g_{CD}). The magnitude of CD and g_{CD} are defined as shown in **Equation 1 and 2**:[1,6,7]

$$CD = A_L - A_R \tag{1}$$

$$g_{CD} = \frac{2 \times (A_L - A_R)}{A_L + A_R} \tag{2}$$

Here, A_L and A_R are the left- and right-handed CP light absorption of the material, which will be measured with a CD spectrometer. The value of g_{CD} is always between -2 and 2, corresponding to 100% right-handed CP light absorption and 100% left-handed CP light absorption, respectively.[6]

Besides the dichroic behavior, CHPs can possess other macroscopic properties such as circularly polarized luminescence (CPL), nonlinear optics, chiral induced spin selectivity (CISS) effect, ferroelectricity, and ferromagnetism.[8] CISS can be characterized via the spin polarization (P_S), which is the degree to which the spin is aligned with a given direction, or in other words, the anisotropy of the spin-polarized currents.[9] CPL is the differential emission of right- and left-handed circularly polarized light, which is correlated with the excited state properties of the chiral systems. In order to understand this difference, the energy levels associated with a CHP can be analyzed, which are shown in **Figure 2**. After an electron is excited from the valence band to the conduction band, the electron relaxes back to the valence band. In the case of radiative relaxation, light is emitted. In CHPs, there are two spin-allowed transitions (Figure 2). For the reduced-dimensional chiral perovskites (RDCP), there will be a difference in spin-polarized emission rate. This is shown by the difference in γ_{exc1} and γ_{exc2}. As a result, in the case of *R*-RDCP, more right-handed CPL (σ^+) will be emitted.[10]

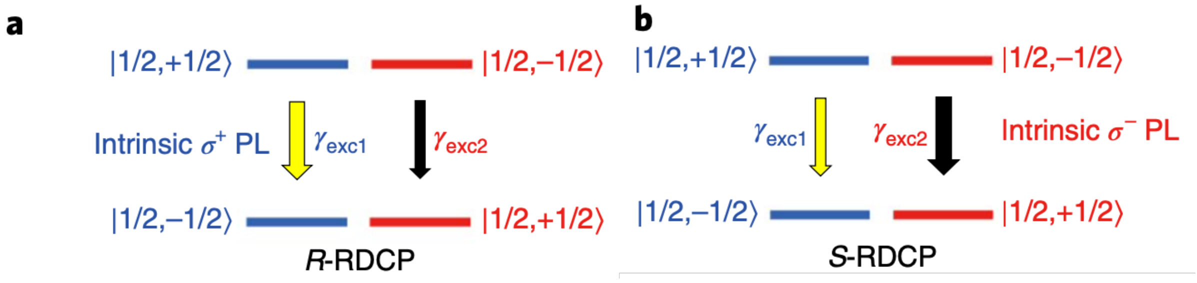

Figure 2. Schematic representation of the conduction and valence band energy levels for the spin-up and spin-down electron of (a) *R*-RDCP and (b) *S*-RDCP.[10]

Circularly polarized light has its applications in sensors, optical storage, and even optical communication. Hence, developing chiral materials that exhibit substantial CD or CPL is of increasing interest. However, in CHPs, the mechanism responsible for CPL still needs to be fully understood.[7] This makes it challenging to optimally design CHPs in a way that leads to high CPL and luminescence dissymmetry factors (g_{lum}), which is deemed essential to fabricate high-performance photonic systems. The intensity of CPL and g_{lum} are defined in **Equation 3 and 4**:

$$CPL = I_L - I_R \tag{3}$$

$$g_{lum} = \frac{2 \times (I_L - I_R)}{I_L + I_R} \tag{4}$$

I_R and I_L are the right- and left-handed CPL intensities measured via a CPL spectrometer. The value of g_{lum} is always between -2 and 2, corresponding to 100 % right-handed CPL and 100 % left-handed CPL, respectively.[11]

In **Figure 3A**, the research on CHPs over the last years is graphically shown. It can be noted that the dissymmetry factors are still limited because of the challenge of finding suitable chiral organic cations that can be incorporated into the HOIPs. However, the progress over the past six years resulted in approximately 30 novel chiral organic cations that can be used to functionalize perovskites.[1] These applied chiral organic cations are mainly limited to commercially available molecules up until now.

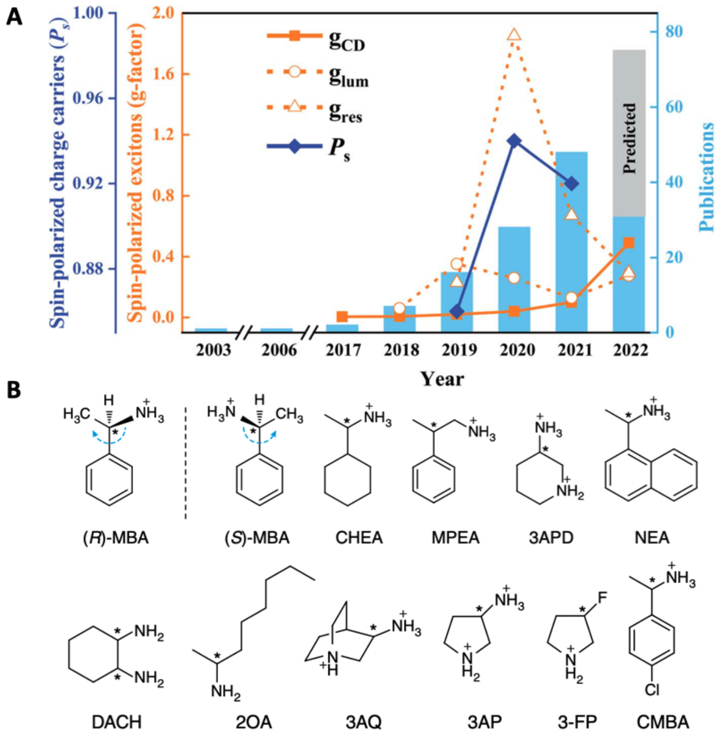

Figure 3. (A) Graphic representation of the total number of published papers in the CHPs field over the past years, the line chart represents the highest value of the dissymmetry factors (g) reported each year. g_{CD} characterizes circular dichroism, g_{lum} characterizes CPL, and g_{res} is the resolution capability of a circularly polarized light photodetector. P_s is the ability to screen spin state electrons as a spin filter layer for a CHP.[1] (B) Chemical structures of the different chiral organic cations that can be used in CHPs: α-methylbenzylammonium (MBA), 1-cyclohexylethylammonium (CHEA), β-methylphenethylammonium (MPEA), 3-aminopiperidine (3APD), 1-(1-naphthyl)ethyl ammonium (NEA), 1,2-diaminocyclohexane (DACH), 2-octylamine (2OA), 3-ammonioquinuclidinium (3AQ), 3-ammoniopyrrolidinium (3AP), 3-fluoropyrrolidinium (3-FP), and 1-(4-chlorophenyl)ethyl ammonium (CMBA).[12]

The chiral organic cations implemented in CHPs consist of an asymmetrical carbon atom with four different substituents and are the main source of asymmetry introduced in the CHPs.[6] Generally, these organic cations contain three components: a headgroup, a chiral center, and an organic core. The head group, mostly a protonated primary ammonium, ionically interacts with the octahedra of the perovskite. The chiral center ensures chirality transfer, which results in inversion symmetry breaking upon the inorganic lattice. The organic cores are comprised of aliphatic chains or (conjugated) rings. Varying the steric hindrance via a change in the molecular structure of the organic core affects the strength of the asymmetric hydrogen bond.[13] **Figure 3B** represents the most used chiral organic cations in CHPs. Every CHP formed by the different chiral organic cations can be used in different applications for their specific chiroptic properties. The chiral ligands α-methylbenzylammonium (MBA), 1-cyclohexylethyl ammonium (CHEA), β-methylphenethyl ammonium (MPEA), 3-aminopiperidine (3APD), 1-(1-naphthyl)ethyl ammonium (NEA), 1,2-diaminocyclohexane (DACH), 2-octylamine (2OA), and 3-ammonioquinuclidinium (3AQ) can be used for CPL detection or as a CPL source. 3-

ammoniopyrrolidinium (3AP), 3-fluoropyrrolidinium (3-FP), and 1-(4-chlorophenyl)ethyl ammonium (CMBA) can be used in ferroelectric applications.[6,12]

HOIPs are self-assembled materials. More specifically, this self-assembly is often induced during solvent evaporation in the annealing step. During solvent evaporation, the interparticle distance decreases, and the inorganic part attracts the organic part via ionic and weak interactions.[14,15] In direct synthesis, the chiral cations, and corresponding inorganic subunits are directly mixed together in a suitable solvent under certain conditions, for example, temperature or pressure, to obtain chiral HOIPs.[7] From these precursors, thin films can be made via spin-coating. Different methods exist to synthesize thin film perovskites, such as a one-step deposition. Here, the precursor will be dripped onto the substrate and spin-coated for 20-60 s at a few thousand rpm spin rate. Afterward, an annealing step is performed to evaporate the residual solvent and complete the crystallization. Another method is hot casting. This method is similar to the one-step method, however, the substrate will first be heated before dripping the precursor onto the substrate. The last method that can be used to synthesize thin films is based on an antisolvent. In this technique, an extra step will be implemented during spinning. Namely, an antisolvent will be dropped onto the spinning film, which removes the solvent and creates a pinhole-free film.[2,16,17] For this project, all CHP thin films were synthesized via the one-step method.

A CD and CPL spectrometer are necessary to measure the chiroptical properties of CHPs. In this work, a CD spectrometer will be obtained by rebuilding the existing CPL spectrometer and validated with reference CHPs and an organic molecule from the literature. Specifically, thin films of (*R/S/Rac*)-[α-methylbenzylammonium)]$_2$PbI$_4$ (MBA$_2$PbI$_4$) and (*R/S/Rac*)-[1-(3-bromophenyl)-ethylammonium]$_2$PbI$_4$ (3BrMBA$_2$PbI$_4$) will be spin-coated on quartz substrates, with Rac representing the racemic mixture. The organic molecule 1(*S*)-(+)-camphorquinone (SCQ) in an ethanol solution was also used as a reference material. Additionally, a home-built CPL spectrometer was employed to measure the CPL from an organic molecule and CHPs to determine the potential artifacts and for validation. Two chiral materials with a known g_{lum} factor were used to measure CPL. The two reference materials are SCQ and CHP thin films of (*R/S/Rac*)-3BrMBA$_2$PbI$_4$. In CPL spectroscopy, the sample can be excited by non-polarized light.[18] The sample will emit an excess of either right-handed circularly polarized (RCP) or left-handed circularly polarized (LCP) light, depending on the absolute configuration (R or S) of the chiral cation employed to form the CHP. This circularly polarized light is converted to linearly polarized light via a quarter-wave plate (QWP) or a photoelastic modulator (PEM). Lastly, this polarized light will be detected with the RCP light on one detector and the LCP light on the second detector. Via the difference in intensities, the dissymmetry factor and the polarization degree (half the dissymmetry factor) can be calculated.[19] Because multiple methods exist to build a CPL spectrometer, variation in the reported dissymmetry factors is almost inevitable due to artifacts. These artifacts can appear from the optical setup, and some examples are a variation of the pump source, a difference in optical path length from the sample to the two different detectors, back-reflection from the polarized beam splitter (PBS), and reflection of polarized excitation light. In addition to the optical setup, artifacts can also arise from the sample. For example, fluorescence anisotropy, which is a linear polarization, originated by matching the orientation of the electronic dipoles and excitation polarization, and reabsorption of CPL.[11,20] Another essential aspect that can give an artifact is the time delay between two measurements from the same sample, leading to partial sample degradation or a drift in the excitation light intensity. Both effects change the luminescence intensity in the spectrum from the second measurement, thus resulting in CPL artifacts.[11] In addition to examining and eliminating artifacts, a home-built setup offers another advantage: its lower cost than a commercial CPL spectrometer.[21] Besides these artifacts from the optical setup and the sample, there is another challenge for CHPs: the measured CPL of the currently developed CHPs decreases if the temperature increases.[18,20] Therefore, there is a need to find novel chiral organic cations that have a high CPL at room temperature. Finally, the sensitivity of the home-built CPL spectrometer must be high enough to measure the CPL of the currently developed CHPs.

In many applications, RCP and LCP light needs to be detected. In the case of normal photodetectors, it is not possible to distinguish the two. Therefore, conventional CPL detection consists of polarizers and quarter-wave plates, which is complex and expensive.[12,17] Furthermore, via the use of polarizers, there will be a loss of 50 % in light intensity.[22] Accordingly, subsequent to building a CD and CPL spectrometer in this project, two photodetectors will be prepared from the reference CHPs. Additionally, a standard external quantum efficiency (EQE) setup will be used to measure the photoresponsitivity of the photodetectors.

2 Results and discussion

2.1 Chemical compositions and optical properties of the chiral hybrid perovskite thin films

To prove whether the chiral perovskite thin films were formed, XRD and UV/Vis measurements were performed. In **Figure 4**, the XRD diffractograms and the absorption spectra of the CHPs are shown with the chemical structure of their corresponding chiral amine. UV/Vis absorption measurements were used to determine the formation of the 2D perovskites (**Figure 4C and F**). Here, it can already be concluded that the 2D perovskites are formed since, for 2D iodide perovskites, the excitonic absorption is around 500 nm. Furthermore, the excitonic band positions of the (*R/S/Rac*)-MBA_2PbI_4 thin films are nearly identical: 505 nm for the R- and the racemic sample and 501 nm for the S-enantiomer, matching closely with the literature values.[23] For the $3BrMBA_2PbI_4$ thin films, the excitonic band for the R/S enantiomers is at 488 nm and for the racemic version, the excitonic band is situated at 499 nm. This position of the excitonic bands corresponds to the values obtained from the literature. Also, the blue shift between the chiral and racemic perovskite is approximately 56 meV and results from stronger structural distortion caused by the chiral organic cations in the *R/S*-3BrMBA$_2$PbI$_4$.[18] From the XRD patterns, **Figure 4B and E**, the crystallinity of the thin films was determined. Here, the planes of the crystals are parallel to the substrate surface. Additionally, for the synthesized MBA$_2$PbI$_4$ thin films, it can be noted that besides the formed 2D perovskite, a small amount of impurity was also present in the thin film, as can be seen from an additional set of peaks (**Figure S1**). This impurity is due to the formation of a one-dimensional (1D) perovskite phase, MBAPbI$_3$.[18,23]

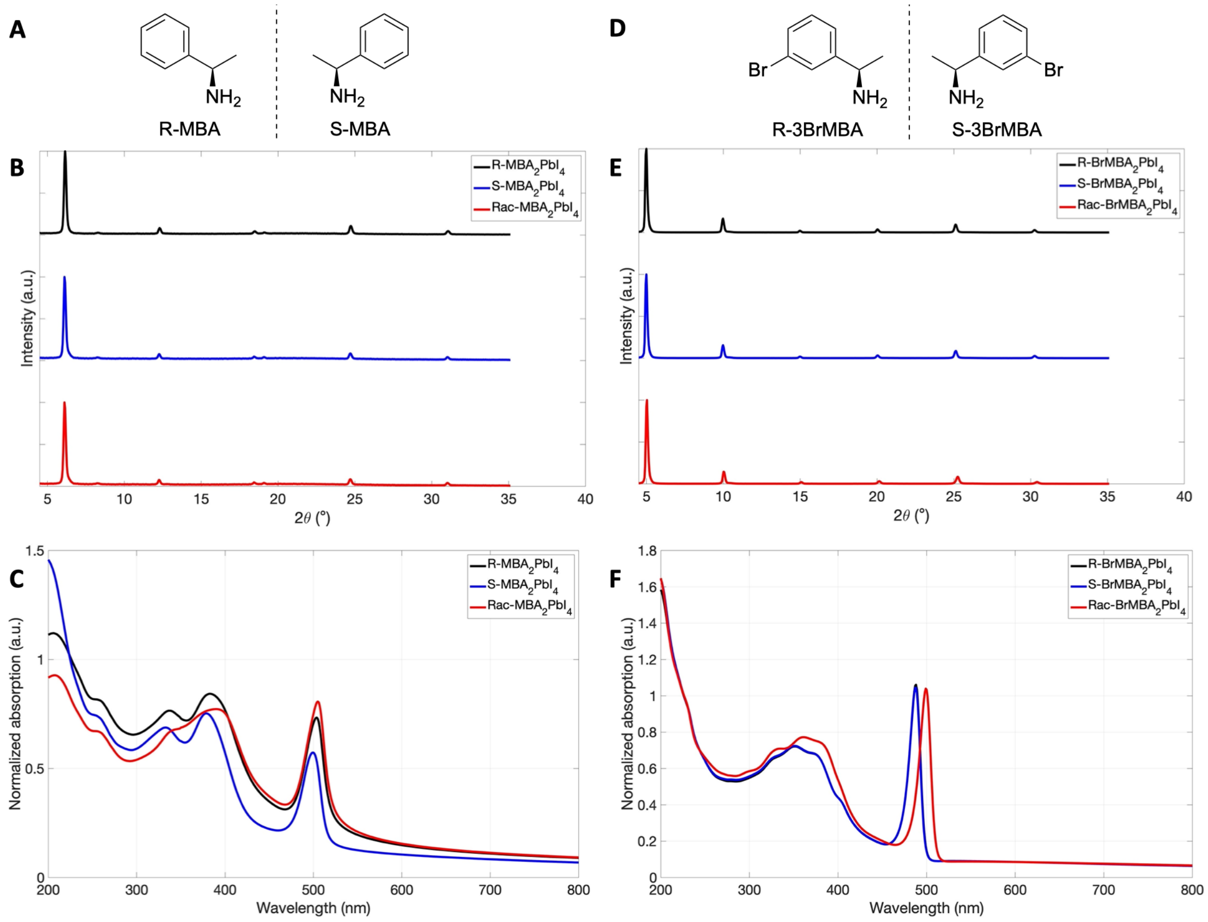

Figure 4. XRD patterns and absorption spectra of two different CHPs with their representing chiral organic cation. (A) Chemical structures of chiral organic enantiomers (*R/S*)-MBA. (B) XRD patterns of the (*R/S/Rac*)-MBA$_2$PbI$_4$ thin films. (C) Absorption spectra of the (*R/S/Rac*)-MBA$_2$PbI$_4$ thin films. (D) Chemical structures of chiral organic enantiomers (*R/S*)-3BrMBA. (E) XRD patterns of the (*R/S/Rac*)-3BrMBA$_2$PbI$_4$ thin films. (F) Absorption spectra of the (*R/S/Rac*)-3BrMBA$_2$PbI$_4$ thin films.

2.2 Setup of the circular dichroism spectrometer

The originally made CPL setup was rebuilt into a CD spectrometer. A schematic view is shown in **Figure S2**. Herein a white light source (LDLS EQ-99X-FC-S) was used, with a lens and slit collimating this unpolarized light. This collimated light then moved through a linear polarizer (Edmund optics High Performance Glass Linear Polarizer) to obtain linearly polarized (LP) light. This LP light was converted into circularly polarized light via a quarter-wave plate (Thorlabs AQWP05M-600). Finally, this circularly polarized light was passed through the sample and was detected on one detector (Avantes AvaSpec-3648USB2-RM). Since this measurement is only a transmission measurement, **Equation 5** was used to convert to calculate the magnitude of the circular dichroism.

$$CD = log\left(\frac{I_R}{I_L}\right) \tag{5}$$

I_R and I_L are the transmitted light intensities for RCP and LCP light, respectively.

Finally, the CD spectrometer was read out and the QWP was automatically rotated using a LabVIEW program. The only parameters that were entered into the LabVIEW program to perform a CD measurement are: the integration time (the time to perform one measurement), the number of averages of one measurement (number of observations per measurement, the total signal is averaged out over these observations), the number of measurements per orientation of the QWP, and the sample orientation (front or back side of the film). When the CD measurement was complete, the obtained data was saved as a text file, and next, the CD and g_{CD} spectra could be plotted in Matlab or Microsoft Excel.

2.3 Circular dichroism spectroscopy

First, verifying that the setup generates CP light to illuminate the sample is essential. To confirm this, two linear polarizers and two QWPs were used (**Figure S3**). By rotating one of the two QWPs, the polarization was reversed and measured on the other detector. In **Figure S4**, the measured intensities of the polarized light are shown, and it can be concluded that there is a generation of circularly polarized light if the QWP is at 45° or 135°.

Now that the generation of CP light is confirmed, the home-built CD spectrometer is validated using chiral materials, such as 1(*S*)-(+)-camphorquinone (SCQ) in an ethanol solution and CHP thin films of (*R/S/Rac*)-MBA_2PbI_4 and (*R/S/Rac*)-$3BrMBA_2PbI_4$. Firstly, the SCQ sample was measured through the CD setup. The results showed that the shape of the CD spectrum (**Figure S5A**) agrees reasonably well with the literature. However, the absolute value of CD is overestimated and mainly arises from the high solution concentration. Besides to make the results concentration independent, the dissymmetry factor could be calculated (**Figure S5B**). It can be concluded that between 400 and 500 nm, the g_{CD} spectrum agrees reasonably well with the literature.[24] Above 500 nm, the spectrum is incorrect, mainly due to artifacts still present. Where this specific artifact stems from is unknown at this moment. Next, the two different CHP thin films were measured to analyze the setup further. In thin films, linear dichroism (LD) and linear birefringence (LB) occur due to thin films being anisotropic. As a result, the observed CD is not genuine. Di Bari et al. observed a sign inversion in CD values when flipping thin films, which indicates that LD or LB changes in sign.[25] Now, to eliminate the LD and LB contributions, CD was calculated by averaging the CD obtained from the front and back side of the film (**Equation 6**). For the CHP thin films, the 2D CHP films have less local anisotropy than the zero-dimensional (0D) and 1D, resulting in a lower LD and LB contribution. However, this elimination method is also used for the 2D CHP films to ensure the measured CD is genuine.[26,27]

$$CD_{Genuine} = \frac{1}{2}(CD_{Front} + CD_{Back}) \tag{6}$$

Where $CD_{Genuine}$ is the real CD value, CD_{Front} and CD_{Back} are the measured CD values from the front and back side of the thin film, respectively. **Figure S6A** shows the genuine CD values. The CD spectra showed that the excitonic peak for the R and S enantiomer is not inverted, as would be expected. Furthermore, the CD spectrum of the racemic mixture should present a baseline value while there is still a signal present at the excitonic peak wavelength with our home-built setup. For the $3BrMBA_2PbI_4$ films (**Figure S6B**) the excitonic peak is inverted for the R and S enantiomer. However, the absolute value of the excitonic peak is much higher according to the literature (approximately 30 mdeg).[18] It can be concluded that the setup picks up contributions from the regular absorption of the 2D perovskite. The exact reason for this artifact is still unknown, but one reason could be the lamp's instability. To potentially solve this problem, more measurements were taken in an attempt to average out the instability of the source. Nevertheless, by increasing the number of repeat measurements, the issue was not solved, and it was observed that during this time, the thin film started to degrade due to extended exposure to the light. Furthermore, it is certain that the synthesized MBA_2PbI_4 films do exhibit CD since they were also measured using a commercial CD spectrometer from JACSO by collaborators (**Figure S7**).

2.4 Setup of the circularly polarized luminescence spectrometer

The home-built spectrometer is based on the setup described by Mackenzie et al. as a solid-state CPL spectrometer and a schematic view is given in **Figure S8**.[28] Instead of using both a beam splitter and linear polarizers, a PBS was used since it includes both functions. To perform such a CPL measurement, the sample was excited by a pulsed laser (Thorlabs NPL35C) with a pulse length of 260 ns and pulse energy of 650 nJ, and the luminescence collimated by a lens. This allowed sufficient luminescence to pass through the QWP (Thorlabs AQWP05M-600), which converted the circularly polarized luminescence to linearly polarized luminescence. This linearly polarized light was split through the PBS (Thorlabs CCM1-PBS251/M), and the horizontally polarized light (or LCP light) was detected on detector I_L and the vertically polarized light (or RCP light) on detector I_R. Important here is that the fast axis of the QWP was at 45° from the horizontal axis of the setup. In addition, if the QWP orientation was set to 315°, the RCP light was measured on detector I_L, and LCP light on detector I_R. Finally, both detectors (Avantes AvaSpec-3648USB2-RM) simultaneously detected these two linearly polarized light beams.

Since the QWP could be rotated via a rotation mount (Thorlabs PRM1), it was possible to use different configurations to perform a CPL measurement. The two configurations that were used are space separation, and space and time separation, **Figure S9** shows the two measurement configurations on the setup. In the space-separated configuration, the orientation of the QWP remained at 45°, and in the space and time-separated configuration, two measurements were performed. One measurement where the QWP was at 45° and one measurement where the QWP was at 315°. By using the space and time separation method, **Equation 3 and 4** changed to **Equation 7 and 8**.

$$CPL = I_L - I_R + I'_L - I'_R \tag{7}$$

$$g_{lum} = \frac{2 \times (I_L - I_R + I'_L - I'_R)}{I_L + I_R + I'_L + I'_R} \tag{8}$$

Here, I_R and I_L are measured with the QWP at 45°, and I_R' and I_L' are measured with the QWP at 315°. Using the space and time separation method, some artifacts from the optical setup, like the variation of the intensity of the pulsed laser, are eliminated.[20] Therefore, this method should result in more reliable CPL values than the space separation configuration. As a final point, the g_{lum} factor is typically in the order of 10^{-3}. Thus, the difference between I_R and I_L is very small. Consequently, the setup must be aligned so that both luminescence spectra have almost the same height, or I_R and I_L need to be very close to one another. Otherwise, incorrect CPL values will be calculated because the luminescence spectra obtained by one of the detectors will always remain larger than the spectra obtained by the other detector.

Finally, the CPL spectrometer was read out, and the QWP was automatically rotated using a LabVIEW program. The code was constructed in a way that it required a calibration before a measurement could be started. After calibration, the integration time, the number of averages of one measurement, and the number of measurements per orientation of the QWP could be set to perform a CPL measurement. When the measurement was done, the obtained data was saved as a text file, and next, the CPL and g_{lum} spectra were plotted in Matlab or Microsoft Excel.

2.5 Circularly polarized luminescence spectroscopy

Two chiral materials with a known g_{lum} factor were used to determine potential artifacts and validate the home-built CPL spectrometer. Namely SCQ and the CHP thin films (*R/S/Rac*)-$3BrMBA_2PbI_4$, with the latter possessing a relatively large photoluminescence quantum efficiency (39 %) and a high degree of CPL according to literature (g_{lum} = 1.04 for single crystals).[18] The first measurements were taken with an achiral material, a thin film of perylene orange, to analyze whether no CPL is erroneously detected for an achiral material and which artifacts can already be examined and eliminated. One artifact already apparent from the obtained spectrum was the wavelength mismatch between the two detectors. **Figure S10** shows the luminescence spectrum of perylene orange measured from the two detectors. Because this mismatch is very small, approximately 1 nm, a zoom-in on one of the luminescence peaks is used to visualize this mismatch (**Figure 5**). A calibration lamp (Ocean Insight HG-2 Mercury-Argon Wavelength Calibration sources) was used to correct this wavelength mismatch. Here, the sample was replaced by the calibration lamp and collimated via a lens. Next, this light was passed through the QWP and detected on the two detectors via the PBS. Usually, The entire setup would be calibrated by performing such a calibration measurement, resulting in more reliable CPL results. However, the setup artifacts made the atomic emission lines broad and noisy. This made it difficult for the LabVIEW program to identify the number of peaks and correctly calibrate the detectors. Therefore, only the two spectrometers/detectors were calibrated instead of the whole setup to obtain a suitable identification of the number of peaks via the LabVIEW program.

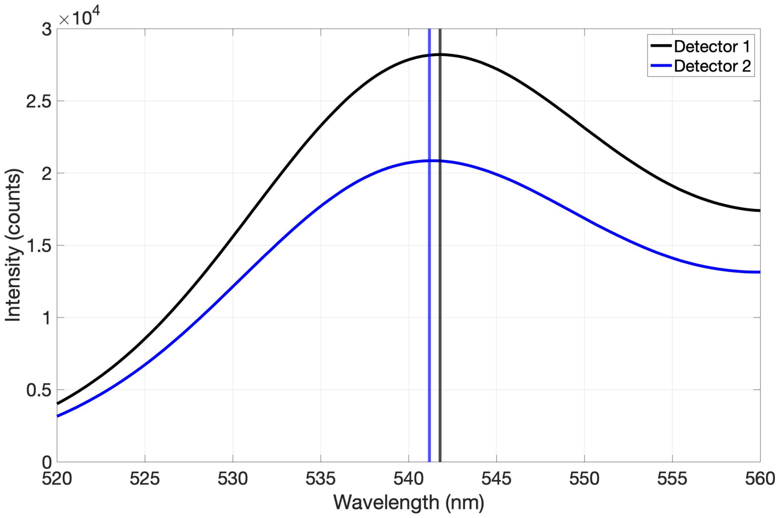

Figure 5. A zoomed-in right- and left-handed photoluminescence spectrum (detector 1 and detector 2, respectively) of a perylene orange thin film measured via the space-separated method under 450 nm excitation. The vertical black and blue lines indicate the wavelength mismatch obtained via the maxima of the two peaks.

2.5.1 Camphorquinone

The luminescence spectra of SCQ are displayed in **Figure S11**. It presents a broad band, and in contrast to the literature, the obtained spectra contained only one broad maximum, which could be due to the high concentration of SCQ in the solution. The first studies were the two measurement configurations space separation, and space and time separation. **Figure 6A** shows the g_{lum} factor measured via these two measurement configurations. It can be noted that the g_{lum} factor measured via space separation gives an overestimation ($g_{\mathrm{lum}} = 0.5$) compared to the value acquired from the literature (see **Figure S12**), which has a maximum of approximately 0.015 at a wavelength of 490 nm. This substantial difference arises mainly from the optical unbalance, such as the alignment of both detectors of the home-built setup. To decrease these artifacts, the space and time-separated configuration was used. At this moment, the g_{lum} factor, see **Figure S13**, is closely in line with the results obtained in the literature. Only the signal obtained below 500 nm does not match the spectra obtained from the literature.[20] Therefore, the CPL spectrum (**Figure S14**) was analyzed to understand the source of this problem. Here, it can be noted that below 500 nm the CPL is negative, which is an effect from the reabsorption of the CPL by the sample.[11]

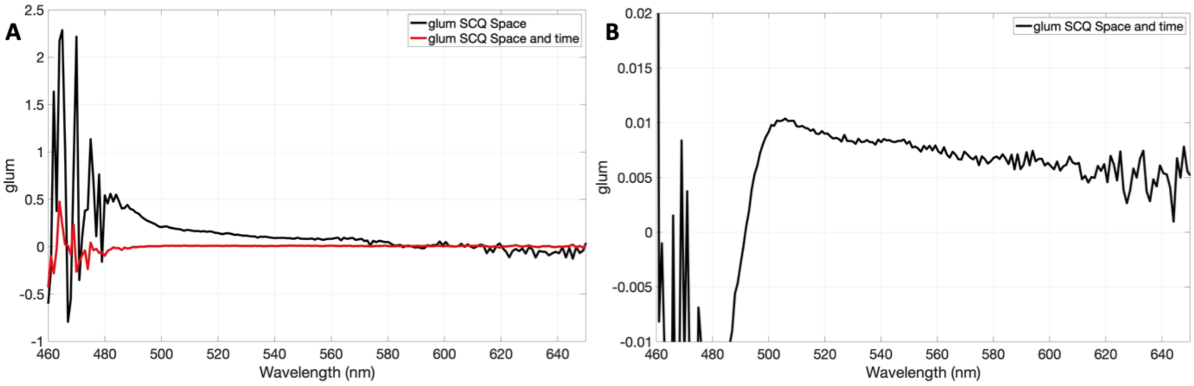

Figure 6. Measured g_{lum} of SCQ under 450 nm excitation. (A) In black, the g_{lum} spectrum obtained via the space separation method, and in red, the spectrum obtained via the space and time separation method. (B) g_{lum} spectrum via the space and time-separated method with 20 measurements per orientation of the QWP.

However, because of the noise, as seen in Figure S14, 20 measurements were taken instead of 10 measurements per sample and orientation of the QWP. After this modification, **Figure 6B** shows the obtained g_{lum} factor, but the reabsorption artifact is still present and needs to be optimized. One way to rule out this artifact is by measuring g_{lum} for a concentration series of SCQ in solution.[11] This could not be performed due to lack of time.

At last, to determine the reproducibility of the CPL setup, the setup was converted again into a CPL setup after first converting to the CD setup, and CPL measurements were again performed on the SCQ sample. **Figure S15** shows these different measurements, where measurements 1 and 2 were performed before the conversion to CD, and measurements 3 and 4 afterward. From this, it can be noted that the results are relatively similar. In addition, in the last measurement more noise was present than in the other measurements. In this last measurement, multiple orientations were used of the QWP outside the usual 45° and 315°. Thus, this noise may indicate that a slight difference in the spectrum may occur if measured at the different orientations of the QWP.

2.5.2 Chiral hybrid perovskite

The chiral hybrid perovskites were only measured using the space and time separation configuration. The first synthesized thin films were too thin to obtain high-intensity luminescence at an integration time of 50 ms. Consequently, two synthesis techniques were used to obtain thicker thin films. The first method used spin-coating at a lower rotation speed, namely 1000 rpm instead of 2000 rpm, with the same concentration of the CHP precursor. The second method was via drop-casting, where the CHP precursor was cast on a glass substrate, followed by the evaporation of the solvent. In this case, a thicker thin film was obtained, but the uniformity of the film was decreased, which may result in increased scattering effects.

The RCPL and LCPL of the spin-coated and drop-casted CHP thin films are shown in **Figure S17 and S18**. The spectra showed a redshift when compared to the literature. The observed redshift can be attributed to the presence of scattered light, which is influenced by the characteristics of the measuring apparatus. Accordingly, it is plausible that this redshift is an artifact originating from the misalignment of the lenses within the setup.[29] From these luminescence spectra, the CPL could be calculated, using **Equation 7**, as shown in **Figure 7**. It can be noted that the setup seems to detect more RCP light from both *R*-3BrMBA$_2$PbI$_4$ and *S*-3BrMBA$_2$PbI$_4$ thin films (**Figure 7A**). For the *R*-3BrMBA$_2$PbI$_4$ thin film, this is expected since it will emit more RCP light because of its chirality. But for *S*-3BrMBA$_2$PbI$_4$, it should be the other way around. The reason for this anomaly is unclear at this moment, and further research is necessary to understand this error. Finally, it can be noted that the setup also seems to detect non-zero CPL from the racemic thin film. A possible cause may be that at the position of excitation, more *S*-3BrMBA$_2$PbI$_4$ is prevalent due to phase-separation. Another reason could be the reabsorption of CPL, which can give rise to the detection of a non-zero CPL value for non-CPL active materials. A way to solve the first issue is by measuring at different positions on the thin film. The second problem can be solved by making a thickness series to analyze at which threshold the reabsorption of CPL is negligible.[11]

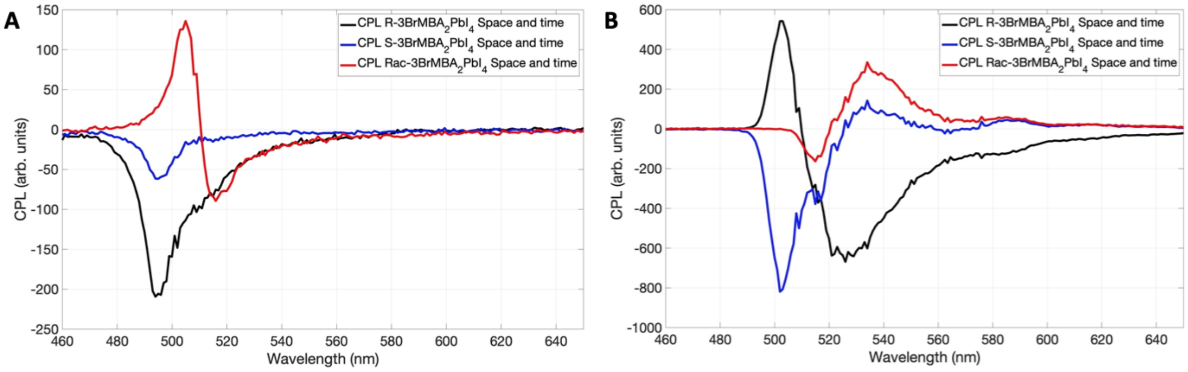

Figure 7. Measured CPL spectra of the $3BrMBA_2PbI_4$ thin films via the space and time separated method under 450 nm excitation, thin films made via (A) spin-coating and (B) via drop-casting.

The obtained CPL from the thin films made via drop-casting is shown in **Figure 7B**. Usually, the R enantiomer should emit more RCP light than LCP light, but the reverse effect is observed below 520 nm. A plausible reason is the reabsorption of CPL, which leads to attenuated CPL intensity or even bisignate CPL.[11] Yet, further research is necessary to eliminate this artifact.

3 Chiral hybrid perovskite photodetectors

Lateral photodetectors were prepared using MBA_2PbI_4 and $3BrMBA_2PbI_4$ spin-coated thin films. Current-voltage (I-V) curves were measured to test the performance of the photodetectors. The device architecture consists of the corresponding CHP film deposited on a quartz substrate. A shadow mask with four interdigitating finger structures, with electrode distances equal to 0.05, 0.10, 0.25, and 0.50 mm, was selected to deposit the gold electrodes on top of the thin film (illustrated in **Figure 8A**). For the racemic CHPs, a poor mask was used and as a result, the electrode distances of 0.05 mm were short-circuited. Next, the photocurrent was measured between the electrode fingers. Here, the sample was either exposed under 1 sun A.M. 1.5G illumination or kept in the dark to obtain the light and dark current, respectively. **Figure 8B and C** shows the I-V curves of the CHP photodetectors measured under dark and light irradiation. From these curves, it can be concluded that the CHP photodetectors generate a photocurrent, and the photodetectors are operational. In addition, the I-V curves are straight lines, making the photodetectors exhibit an ohmic behavior. Furthermore, it can be noted that the *R*-$3BrMBA_2PbI_4$ films have a lower resistance (approximately 70 GΩ under dark) compared to the MBA_2PbI_4 films (approximately 80 GΩ under dark). A possible explanation is that the $3BrMBA_2PbI_4$ films have a higher electron mobility. Therefore, the electrons can move more efficiently, which leads to a higher dark current. Another aspect that can be calculated from Figure 8B and C is the light/dark current ratio for the different photodetectors (**Figure S19 and S20**). The light/dark current ratio for the detectors under 10 V bias is approximately 1.5 for the (*R/S*)-MBA_2PbI_4 films and approximately 6.6 for the *Rac*-MBA_2PbI_4 films. For the

$3BrMBA_2PbI_4$ films the light/dark current ratio under 10 V bias is approximately 19.1, 1.0, and 11.0 for the (*R/S/Rac*)-$3BrMBA_2PbI_4$ films, respectively. From these values, it can also be verified that the $3BrMBA_2PbI_4$ films will perform better. This is supposedly due to a higher absorption coefficient but could also be due to higher charge mobility or longer charge life. Finally, the EQE of the photodetectors was measured. Nevertheless, due to the very small final photocurrent around 0.2 nA at a bias of 10 V and lower light intensity of the EQE setup than that of the solar simulator, it was not possible to determine an EQE spectrum of these photodetectors and eventually to determine the photoresponsivity.

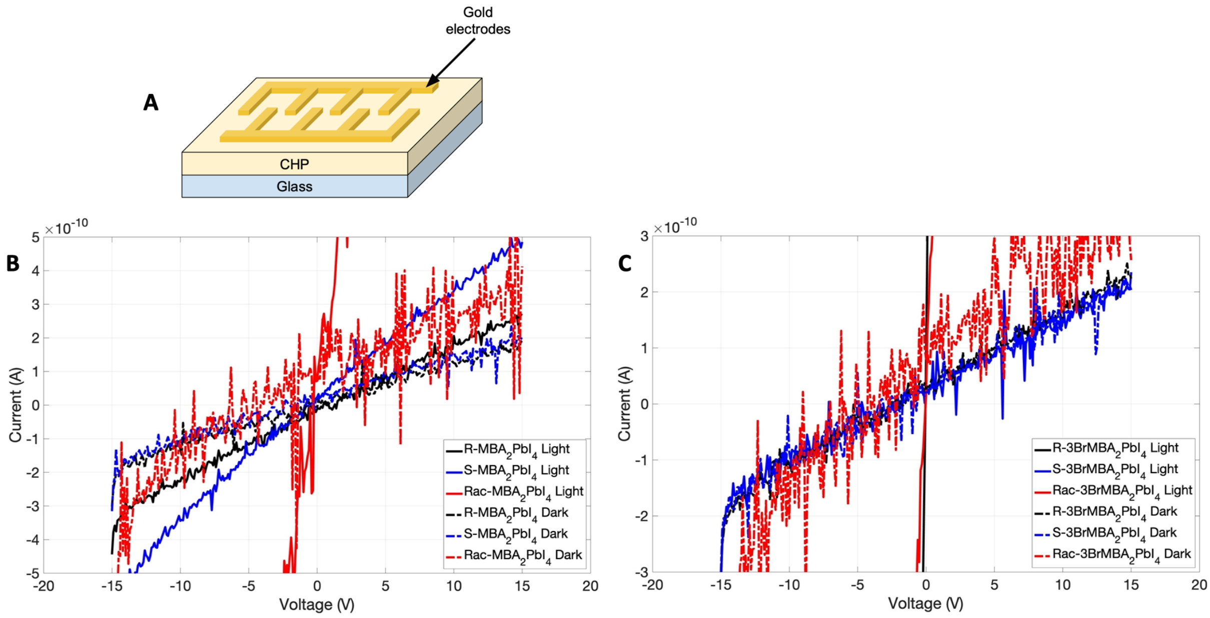

Figure 8. (A) Schematic view of the photodetector consisting of a CHP thin film and a gold electrode. The I-V curves of the photodetector based on (B) (*R/S/Rac*)-MBA_2PbI_4 and (C)(*R/S/Rac*)-$3BrMBA_2PbI_4$, with the electrode distance $L = 0.05$ mm for the R and S enantiomers and $L = 0.10$ mm for the racemic films, under light irradiation and in the dark.

4 Conclusion

In this project, a CD and CPL spectrometer were built and validated with chiral reference materials, such as small organic molecules in solution and CHP thin films. Preliminary measurements were set to determine the responsivity of photodetectors based on CHPs. First, the CD spectrometer was built from the existing CPL spectrometer setup. The results show that it is possible to determine CD from organic molecules in solutions with reasonable accuracy. On the other hand, the artifacts that were already present appear more prominently for the CHP thin films. Furthermore, the CD spectrometer picks up contributions from the regular absorption of the 2D CHP. One potential cause is the lamp's instability, which could be easily solved by taking more measurements per orientation of the QWP. However, the samples start to degrade due to too long light exposure. Other artifacts may arise from the setup or the sample, but the origin is unknown at this moment, so further research is needed to optimize the CD setup. The CPL spectrometer exhibited artifacts as well. The first one is the wavelength mismatch, which could be solved by calibrating the detectors with a calibration lamp. Next, multiple artifacts/anomalies may arise from the optical components. For instance, the instability of the excitation laser, poor setup alignment, and differing optical path lengths for both detectors. To resolve most of the artifacts, the time and space separation method can be used, where the instability of the laser will be canceled out. The results obtained are more consistent with these modifications. Furthermore, other artifacts mostly originate from the sample and were mainly due to the reabsorption of CPL. For now, deviating g_{lum} values are obtained because of an attenuated CPL intensity, and a correction equation needs to be derived to correct the CPL spectra. Another way to rule out this artifact is by measuring g_{lum} for a concentration series of samples in solution or a thickness series for thin films. As a result, measuring the samples' CD before CPL measurements is necessary to check for CPL reabsorption. Finally, the reference CHPs were made into photodetectors. From the I-V curves, it can be noted that the obtained photocurrent is relatively small, namely around 0.2 nA, even with a bias of 10 V. Light/dark current ratios of approximately 1.5 for (R/S)-MBA_2PbI_4, and 19.1 for (R/S)-$3BrMBA_2PbI_4$ were obtained. From these results, it can be concluded that the (R/S/Rac)-$3BrMBA_2PbI_4$ devices perform better than the (R/S/Rac)-MBA_2PbI_4 devices. This is supposedly due to a higher absorption coefficient but could also be due to higher charge mobility or longer charge life. Moreover, because of the low absolute current, the external quantum efficiency of the photodetectors could not be determined. A solution to this is to make the CHP film thicker so that more light can be absorbed.

To continue this work, the artifacts of both spectrometers need to be improved first. In both cases, the QWP can be substituted with a photoelastic modulator, resulting in a tenfold increase in setup sensitivity. Furthermore, the light source needs to be replaced. A more stable lamp or a monochromator can be utilized for the CD spectrometer. At the same time, a laser or monochromatic light source with a lower wavelength and higher light intensity must be employed for the CPL setup to excite various chiral samples, such as 1D CHPs. In addition, the light source must emit unpolarized light, such that it will not already have preferential luminescence in either of the two polarized states. After this optimization, chiral materials with high g_{CD} or g_{lum} can be measured for further investigation in the artifacts arising from the CD and CPL setup.

5 Experimental Methods

5.1 Salt formation of the chiral organic amines

For the salt formation, the reagents hydroiodic acid (57 wt%) and *Tri*-*n*-butyl phosphate (98%) were bought from Fisher Scientific. The chiral amines *S*-MBA and *R*-MBA were purchased from Fluorochem and *R*-3BrMBA and *S*-3BrMBA from BLD Pharm.

5.1.1 S-(-)-1-Phenylethylammonium iodide and R-(+)-1-Phenylethylammonium iodide

8.376 mmol of *S*-MBA (or *R*-MBA) was added together with 20 mL dichloromethane (DCM) and a stirring bar to a 50 mL 3-neck round-bottom flask (RBF). The mixture was flushed with Ar (g). Hydroiodic acid (57 wt%) was extracted with 1:10 (V/V) tributylphosphate:$CHCl_3$ to remove impurities. Immediately after the third extraction, the hydroiodic acid fraction (bottom) was let off, and 8.795 mmol was added to the DCM mixture. The mixture was flushed with Ar (g) and left to react in the dark overnight at room temperature. The contents were transferred to a 500 mL RBF, the solvent was evaporated and 400 mL of ether was added. This was sonicated until the salt precipitated, after which it was filtered. The salt was dried under a high vacuum overnight.

5.1.2 S-1-(3-Bromophenyl)ethyl ammonium iodide and R-1-(3-Bromophenyl)ethyl ammonium iodide

5.297 mmol of *S*-3BrMBA (or *R*-3BrMBA) was together with 20 mL DCM and a stirring bar added to a 50 mL 3-neck round-bottom flask (RBF). The mixture was flushed with Ar (g). Hydroiodic acid (57 wt%) was extracted with 1:10 (V/V) tributylphosphate:$CHCl_3$ to remove impurities. Immediately after the third extraction, the hydroiodic acid fraction (bottom) was let off, and 5.560 mmol was added to the DCM mixture. The mixture was flushed with Ar (g) and left to react in the dark for 3 hours. The contents were slowly dropped into 500 mL cold ether, but no precipitation occurred. The solvent was evaporated, and the oil was redissolved in ether. After sonication, a precipitate formed, after which it was filtered and dried under a high vacuum overnight.

5.2 Synthesis of chiral perovskite thin films

The precursor solutions were all prepared starting from an (*R/S*)-MBA iodide salt or (*R/S*)-3BrMBA iodide salt, both with 99.99 % pure PbI_2 (stored in a glovebox) from TCI chemicals.

For the ((*R/S*)-MBA)$_2$PbI$_4$ precursor: 14.9 mg of (*R/S*)-MBA iodide salt (0.2 M) was added together with 13.8 mg PbI_2 (0.1 M) and 300 μL dry *N,N*-dimethylformamide (DMF) in a glass vial. The racemic perovskite was made by adding 7.5 mg of (*R*)-MBA iodide salt and 7.5 mg of (*S*)-MBA iodide salt (0.2 M) together with 13.8 mg PbI_2 (0.1 M) and 300 μL dry DMF in a glass vial. The ((*R/S*)-3BrMBA)$_2$PbI$_4$ precursor was made by: 19.7 mg of (*R/S*)-MBA iodide salt (0.2 M) was added together with 13.8 mg PbI_2 (0.1 M) and 300 μL dry DMF in a glass vial. The racemic perovskite was made by adding 9.9 mg of (*R*)-MBA iodide salt and 9.9 mg of (*S*)-MBA iodide salt (0.2 M) together with 13.8 mg PbI_2 (0.1 M) and 300 μL dry DMF in a glass vial.

The precursor solutions were mixed for one and a half hours at room temperature. Next, these solutions were spin-coated on quartz substrates. These substrates were cleaned beforehand by subsequent 15 minutes sonication steps in DMF, dimethyl sulfoxide (DMSO), H_2O, acetone, and 2-Propanol (IPA). Right before spin-coating, the substrates were treated with UV-ozone for 15 minutes. 40 μL of each chiral perovskite precursor solution was spin-coated in a glovebox under nitrogen atmosphere ($<$ 1 ppm O_2, $<$ 1 ppm H_2O) at 2000 rpm and 2000 rpm s^{-1} for 20 seconds, unless specifically stated otherwise. The films were annealed on a hot plate at 100 °C for 10 minutes in the glovebox. All films were stored under an Ar (g) atmosphere and only brought under an ambient atmosphere for characterization.

5.3 Absorption measurements

Optical absorption measurements were performed between 200 and 800 nm on a Cary 5000 UV-Vis-NIR spectrophotometer from Agilent technologies with a tungsten halogen visible and deuterium arc UV lamp as a light source. A clean quartz substrate was used as a blank for calibration.

5.4 X-ray diffraction measurements

X-ray diffraction was measured at room temperature under an ambient atmosphere on a Bruker D8 Discover diffractometer with a parallel beam geometry using a Göbel mirror and CuK_α radiation with an energy-dispersive one-dimensional detector (Lynxeye).

5.5 CD measurements

CD measurements were performed using a white light source (LDLS EQ-99X-FC-S). A lens and slit collimated this light. This collimated light then moved through a linear polarizer (Edmund optics High Performance Glass Linear Polarizer) in order to obtain LP light from the unpolarized light. This LP light could be converted to CP light via a quarter-wave plate (Thorlabs AQWP05M-600). This circularly polarized light passed through the sample and the transmitted light was detected (Avantes AvaSpec-3648USB2-RM detector).

Three reference materials were used to validate the CD spectrometer. The first reference material is 1(*S*)-(+)-camphorquinone in solution. 1(*S*)-(+)-camphorquinone, see **Figure S23**, was purchased from TCI. CD measurements were carried out on an ethanol solution. Typical concentrations of 100 mM were used. The second and third reference materials were thin films of (*R/S/Rac*)-MBA_2PbI_4 and (*R/S/Rac*)-$3BrMBA_2PbI_4$, see **Figure 4A and D** for the chemical structure of the chiral organic cations. Both reference materials were measured using an integration time of 3 ms, the number of averages per measurement was 200, and 40 measurements were done per orientation of the QWP. The film's front and back sides were measured for the thin films to determine the genuine CD values, which is the average of the CD_{Front} and CD_{Back} values.

5.6 CPL measurements

The home-built setup is based on the configuration described by Mackenzie et al. as a solid-state CPL spectrometer and a schematic view is given in **Figure S8**.[28] However, instead of using both a beam splitter and linear polarizers, a PBS would be used since it includes both functions in one. The sample was excited by a pulsed laser (Thorlabs NPL45C) with a pulse length of 260 ns and pulse energy of 650 nJ to perform such CPL measurements. A lens collimated the luminescence from the sample. This allowed sufficient luminescence to pass through the quarter-wave plate (Thorlabs AQWP05M-600) and convert the circularly polarized luminescence to linearly polarized luminescence. This linearly polarized light was then split through the PBS (Thorlabs CCM1-PBS251/M), and the horizontally polarized light (or LCP light) was detected on detector I_L and the vertically polarized light (or RCP light) on detector I_R. Both detectors are integrated into the spectrometer AvaSpec-3648USB2-RM from Avantes.

Two reference materials were used to validate the CPL spectrometer. The first reference material is a material in solution, namely 1(*S*)-(+)-camphorquinone in ethanol. CPL measurements have been carried out on solution samples by dissolving these molecules in ethanol. Typical concentrations of 100 mM were used. The second reference material is a thin film of (*R/S/Rac*)-$3BrMBA_2PbI_4$, see Figure 4D for the chemical structure of the chiral 3BrMBA. The thin films were synthesized via spin-coating the correct precursor solution at 1000 rpm or via drop-casting. Both reference materials were excited with a pulsed laser (λ = 450 nm, 50 kHz) as specified previously. The integration time was set at 50 ms, the number of averages per measurement was 100, and 10 measurements were done per orientation of the QWP. The number of measurements per configuration was later increased to 20 to enhance the signal-to-noise ratio.

5.7 Synthesis and characterization of the CHP photodetectors

Photodetectors were made by spin-coating thin films of (*R/S/Rac*)-$3BrMBA)_2PbI_4$ precursors (0.2 M) and (*R/S/Rac*)-$3BrMBA)_2PbI_4$ precursors (0.2 M), such as described in the synthesis of chiral perovskite thin films. Electrodes featuring interdigitating finger structures were produced by evaporating 80 nm of gold onto the CHP thin films through a shadow mask. The devices were measured from -15 V to 15 V in 0.1 V increments in the dark and under 1 sun AM 1.5G illumination. The EQE measurements utilized a custom-built setup comprising a Newport Apex illuminator (100 W Quartz Tungsten Halogen lamp) as the light source and a Newport Cornerstone 130° monochromator. The monochromatic light was subjected to a chopper frequency of 135 Hz, and the resulting photocurrent was measured using a Stanford lock-in amplifier. The signal was pre-amplified using a DLPCA-200 amplifier from FEMTO at a voltage of 10 V.

Acknowledgments

I want to thank Aleksandra Ciesielska for guiding me through the experiments where I needed assistance. Also, I would like Dr. Melissa Van Landeghem to ensure my master's thesis was made into an academic format. I would also like to thank Prof. Dr. Wouter Van Gompel and Prof. Dr. Ir. Koen Vandewal for further guidance and for considering topics that could contribute to this master's thesis. This project was a very challenging topic that often involved specified knowledge in chemistry and physics. Due to this, I want to thank you for being able to work on this project, as I learned a lot on an academic and personal level. I would also like to thank both research groups for the pleasant environment and, during the group meetings, for thinking about the problems that arose, even if this subject is not well known to the majority. A special thanks to Dr. Sigurd Mertens for the assistance in the fabrication and characterization of the photodetectors. In addition, I would like to thank Dr. Dorien Baeten, for always being available if there were any issues regarding the master's thesis and the master's degree. Finally, I would like to thank my family and friends for their support throughout my master's degree.

References

(1) Xiao, J. et al. *Journal of Materials Chemistry A* **2022**, *10*, 19367–19386.

(2) Li, X. et al. *Chemical Reviews* **2021**, *121*, 2230–2291.

(3) Wu, H.-S. et al. *Advanced Science* **2022**, *9*, 2104703.

(4) Van Gompel, W. T. M. et al. *Journal of Materials Chemistry C* **2023**, *11*, 12877–12893.

(5) Billing, D. G. et al. *Acta Crystallographica Section E: Structure Reports Online* **2003**, *59*, 381–383.

(6) Pietropaolo, A. et al. *Chem* **2022**, *8*, 1231–1253.

(7) Lu, H. et al. *Nature Reviews. Chemistry* **2022**, *6*, 470–485.

(8) Dong, Y. et al. *Small* **2019**, *15*, 1902237.

(9) Ray, S. C. In *Magnetism and Spintronics in Carbon and Carbon Nanostructured Materials*, Ray, S. C., Ed.; Micro and Nano Technologies; Elsevier: 2020, pp 1–21.

(10) Long, G. et al. *Nature Photonics* **2018**, *12*, 528–533.

(11) Kitzmann, W. R. et al. *Advanced Materials* **2023**, *35*, 2302279.

(12) Long, G. et al. *Nature Reviews Materials* **2020**, *5*, 423–439.

(13) Ding, Z. et al. *JACS Au* **2024**, *4*, 1263–1277.

(14) Liu, J. et al. *Accounts of Chemical Research* **2022**, *55*, 262–274.

(15) Park, G. et al. *Scientific Reports* **2018**, *8*, 4661.

(16) Zhu, H. et al. *ACS Applied Materials & Interfaces* **2023**, *15*, 9978–9986.

(17) Ma, J. et al. *Advanced Materials* **2021**, *33*, 2008785.

(18) Liu, S. et al. *Science Advances* **2023**, *9*, eadh5083.

(19) Zhang, Y. et al. *Matter* **2022**, *5*, 837–875.

(20) Baguenard, B. et al. *Nature Communications* **2023**, *14*, 1065.

(21) On-Line Instrument Systems Inc. CPL Comparison, OLIS CLARiTY https://olisclarity.com/cpl-comparison (accessed 10/15/2023).

(22) Baek, K. et al. *Light: Science & Applications* **2019**, *8*, 120.

(23) Ahn, J. et al. *Materials Horizons* **2017**, *4*, 851–856.

(24) Pandiscia, L. et al. CPL Measurement of Camphorquinone Using CPL-300 Circularly Polarized Luminescence Spectrometer, JASCO Inc. https://jascoinc.com/applications/cpl-measurement-camphorquinone-using-cpl-300-circularly-polarized-luminescence-spectrometer/ (accessed 05/24/2024).

(25) Albano, G. et al. *Materials Chemistry Frontiers* **2017**, *1*, 2047–2056.

(26) Han, X.-B. et al. *Analytical Chemistry* **2023**, *95*, 16201–16209.

(27) Zhang, Z. et al. *Journal of the American Chemical Society* **2022**, *144*, 22242–22250.

(28) MacKenzie, L. E. et al. *Nature Communications* **2020**, *11*, 1676.

(29) Van der Pol, T. P. A. et al. *Advanced Optical Materials* **2022**, *10*, 2102557.

Supporting information

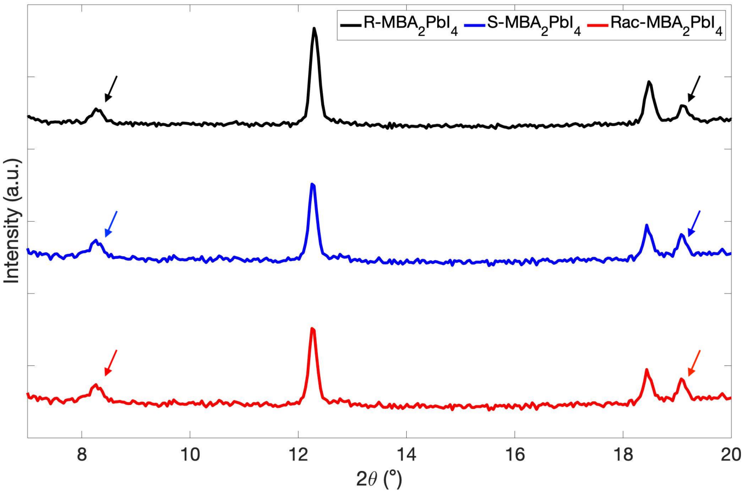

Figure S1. Zoom-in of the XRD patterns of the (*R/S/Rac*)-MBA$_2$PbI$_4$ thin films.

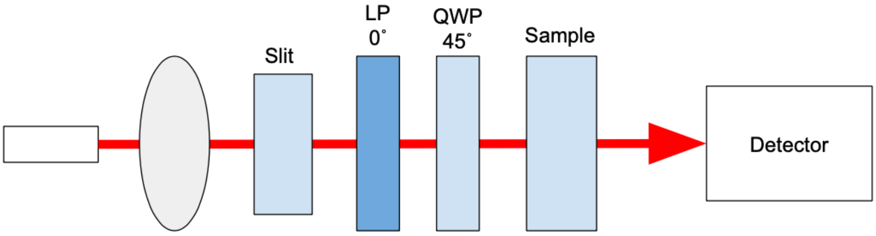

Figure S2. Schematic representation of a CD spectrometer, where a white lamp is collimated with a lens and slit, next circularly polarized light is created via a linear polarizer (LP) and a quarter-wave plate (QWP), and this light is transmitted through the sample to the detector.

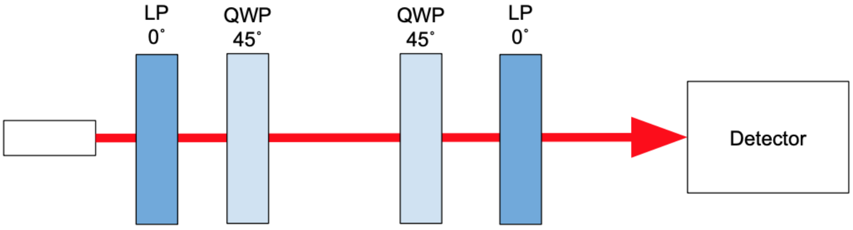

Figure S3. Schematic representation of a setup to verify the creation of CP light, where a white lamp is used. Next, circularly polarized light is created via a linear polarizer (LP) and a quarter-wave plate (QWP). Secondly, This light will be converted back to linear polarized light via a QWP, and depending on the polarization, the light will be stopped or passed through the LP. Finally, this light will be detected via a detector.

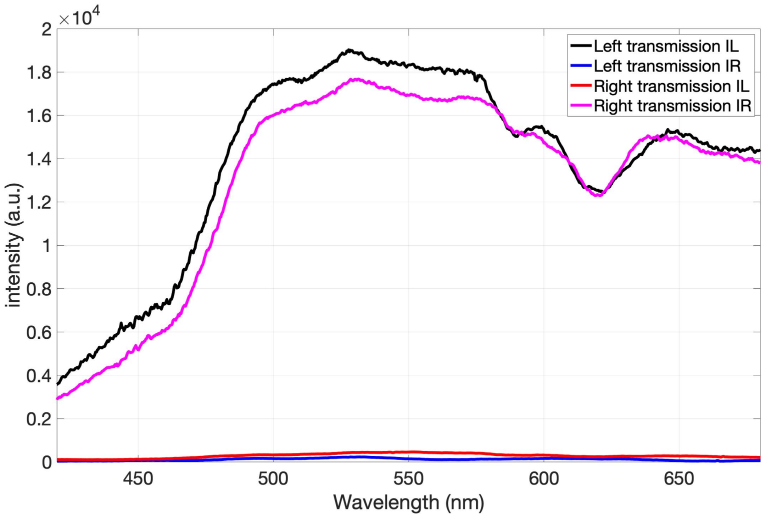

Figure S4. Transmission measurements by creating circularly polarized light via a linear polarizer and QWP, at varied angles, and transformed back to linearly polarized light via another QWP at 45°and a PBS.

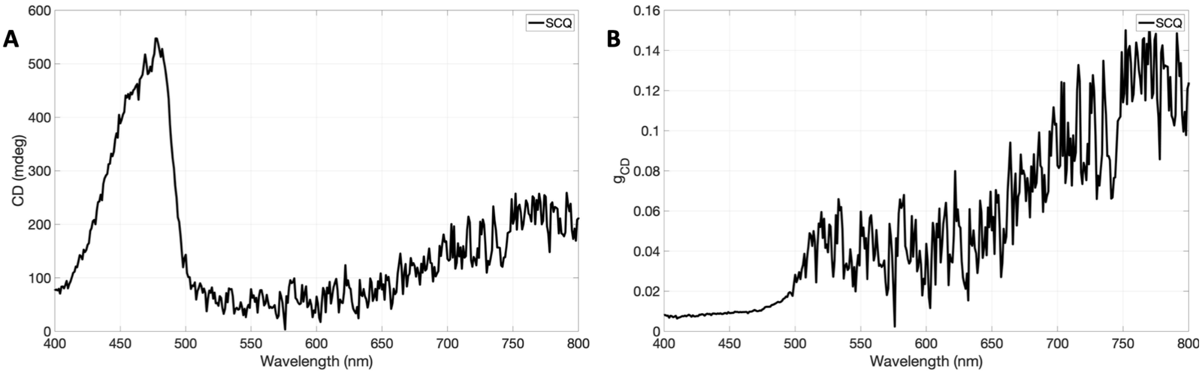

Figure S5. (A) CD and (B) g_{CD} spectra of SCQ with 20 measurements per orientation of the QWP, the orientations of the QWP are: 45°, 135°, 225°, and 315°.

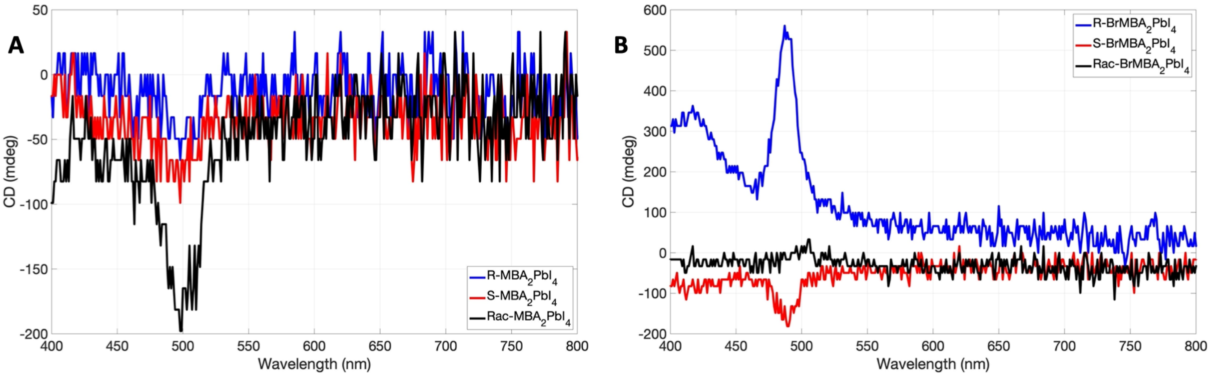

Figure S6. Measured CD spectra of the (A) (*R/S/Rac*)-MBA_2PbI_4 and (B) (*R/S/Rac*)-$3BrMBA_2PbI_4$ thin films.

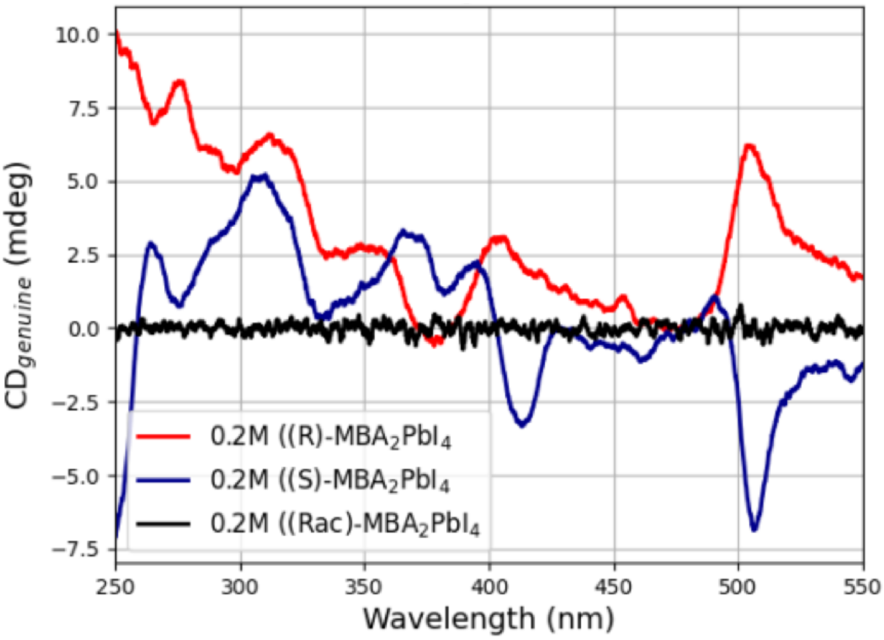

Figure S7. CD spectra of (*R/S/Rac*)-MBA_2PbI_4 thin films measured on a commercial CD spectrometer from JASCO.

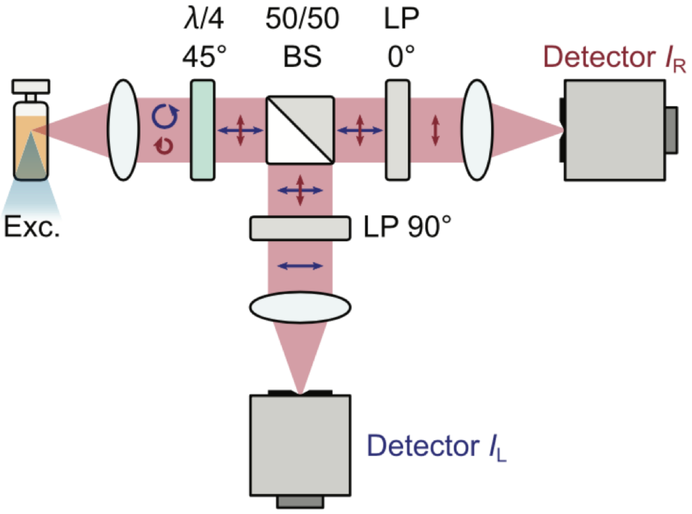

Figure S8. Schematic representation of a CPL spectrometer, where the sample is excited, and the circularly polarized luminescence is linearly polarized by a quarter-wave plate (λ/4). The linear polarized light is split via a beam splitter (BS) and a linear polarizer (LP) so that the correct polarized light is detected on the right detector.[11]

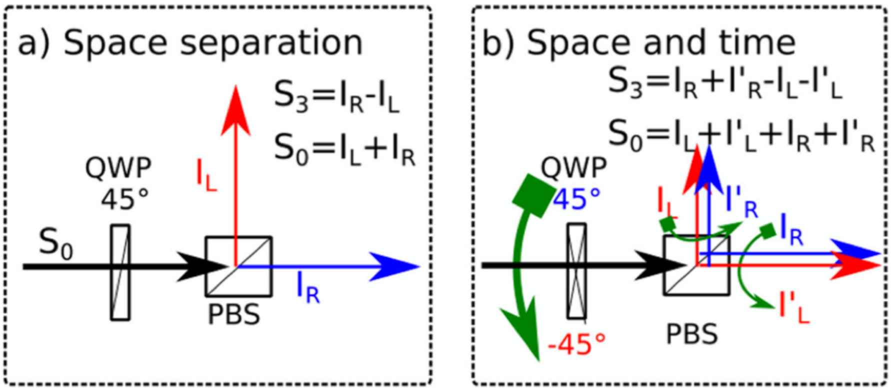

Figure S9. Two measurement configurations for a CPL spectrometer, with (a) one measurement of RCP and LCP at a constant orientation of the QWP, and (b) two measurements of RCP and LCP by rotating the QWP over 90°. Hereby, S_0 is the total intensity and S_3 the opposite of CPL.[20]

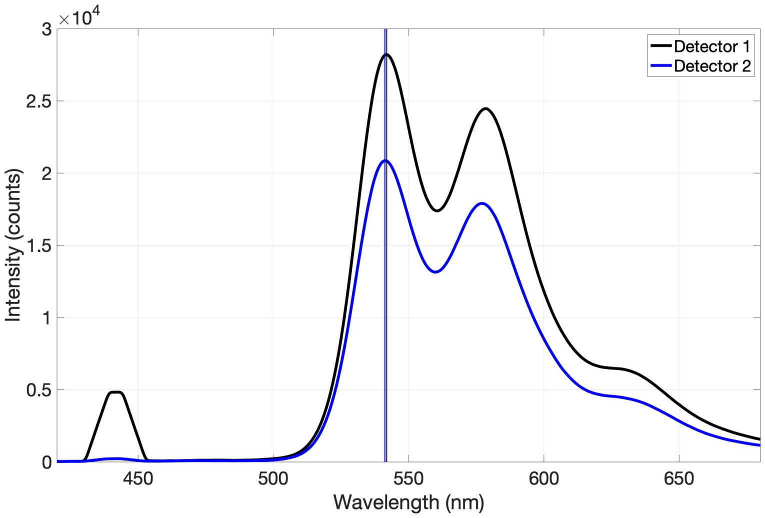

Figure S10. Photoluminescence spectrum of a perylene orange thin film measured via the space-separated method under 450 nm excitation. The vertical black and blue lines indicate the wavelength mismatch obtained via the maxima of the two peaks.

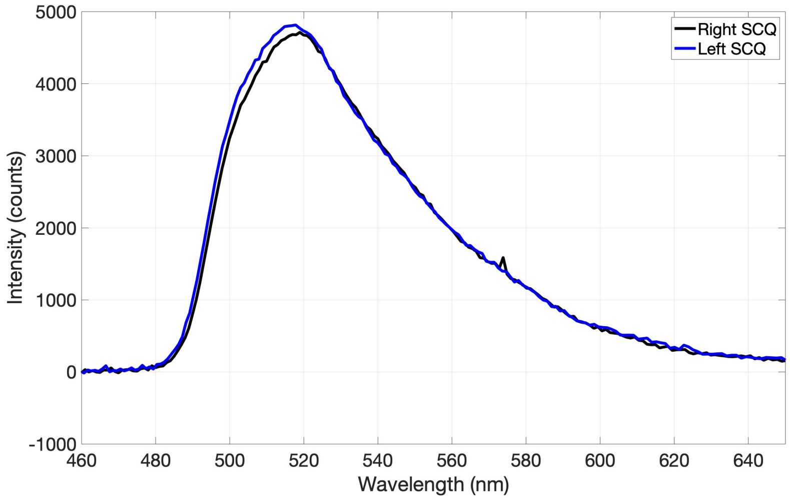

Figure S11. Measured right- and left-handed CPL of SCQ via the space and time separated method under 450 nm excitation and 10 measurements per orientation of the QWP.

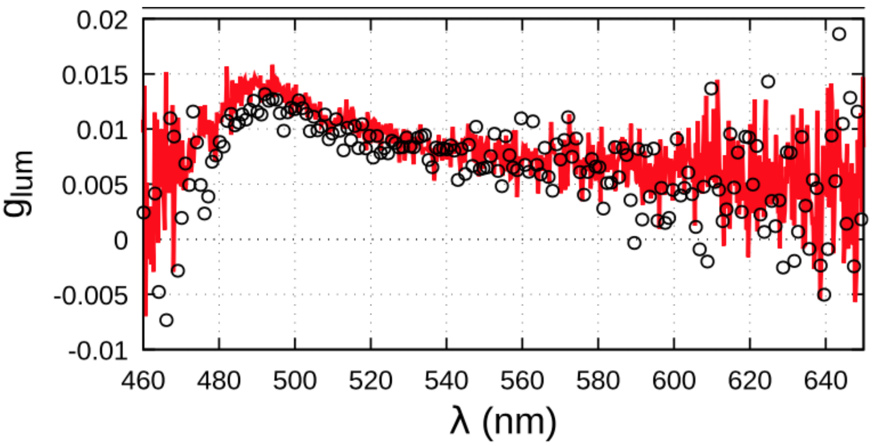

Figure S12. Measured g_{lum} of SCQ from the literature via the space and time separated method under 450 nm excitation. In red is the recorded spectrum with a charge-coupled device (CCD) camera using the space and time separation method. In the black circle, is the recorded spectrum in a step-by-step setup using a PEM+analyser system.[20]

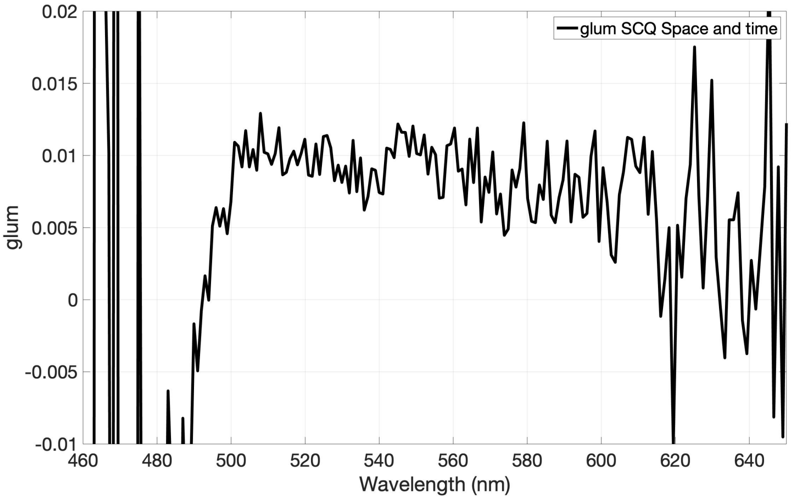

Figure S13. Measured glum of SCQ on our setup via the space and time separated method under 450 nm excitation and 10 measurements per orientation of the QWP.

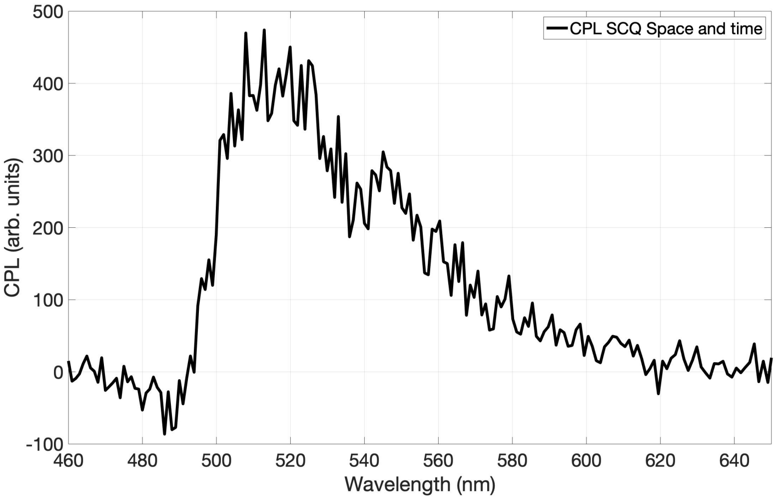

Figure S14. Measured CPL of SCQ via the space and time separated method under 450 nm excitation and 10 measurements per orientation of the QWP.

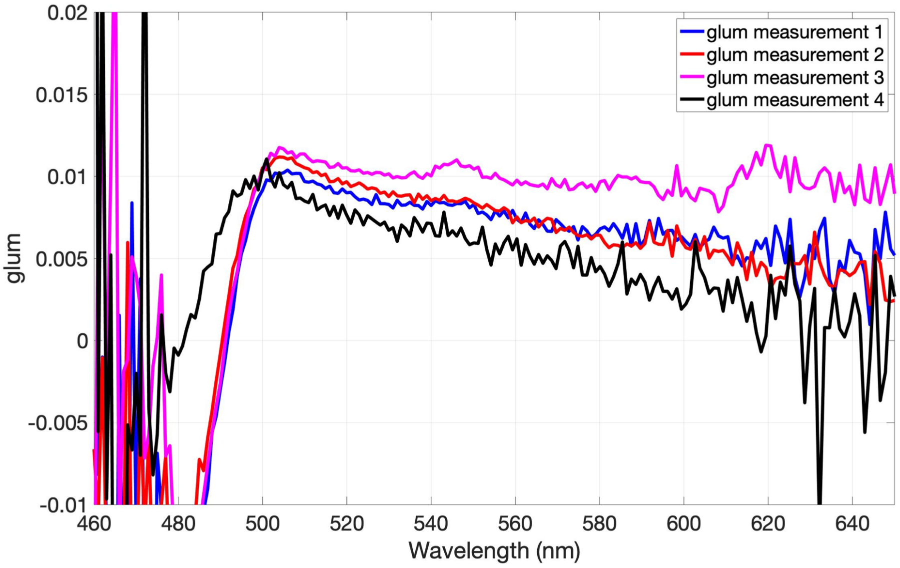

Figure S15. g_{lum} spectra of SCQ measured at different moments during this project. For the first three measurements, the orientations of the QWP are 45° and 315 °, and for the last measurement (4), the orientations of the QWP are 45°, 135°, 225°, and 315°. All spectra are obtained via the space and time separation method.

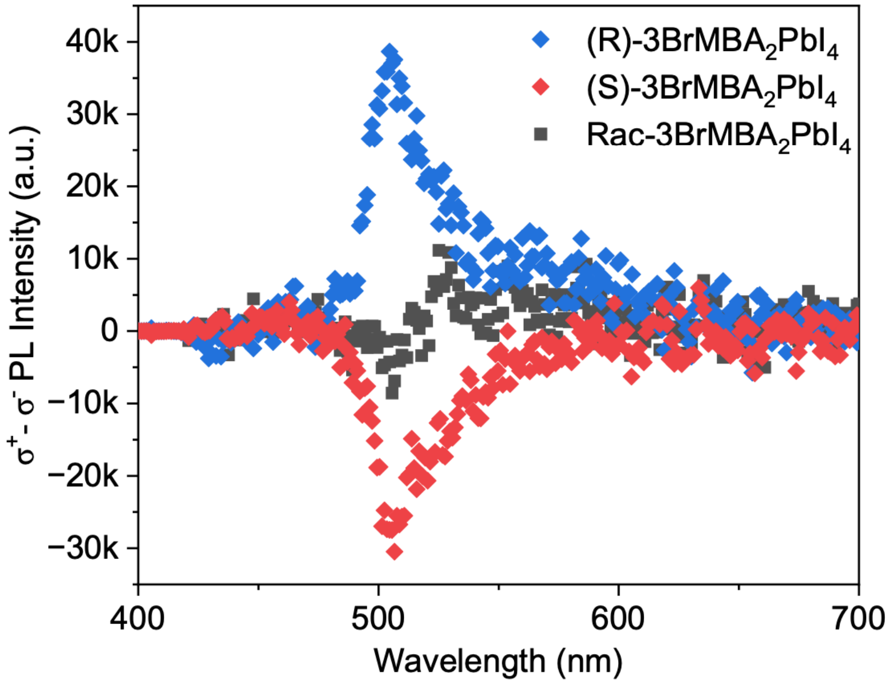

Figure S16. Difference in photoluminescence intensities between right-handed (σ^+) and left-handed (σ^-) detections.[18]

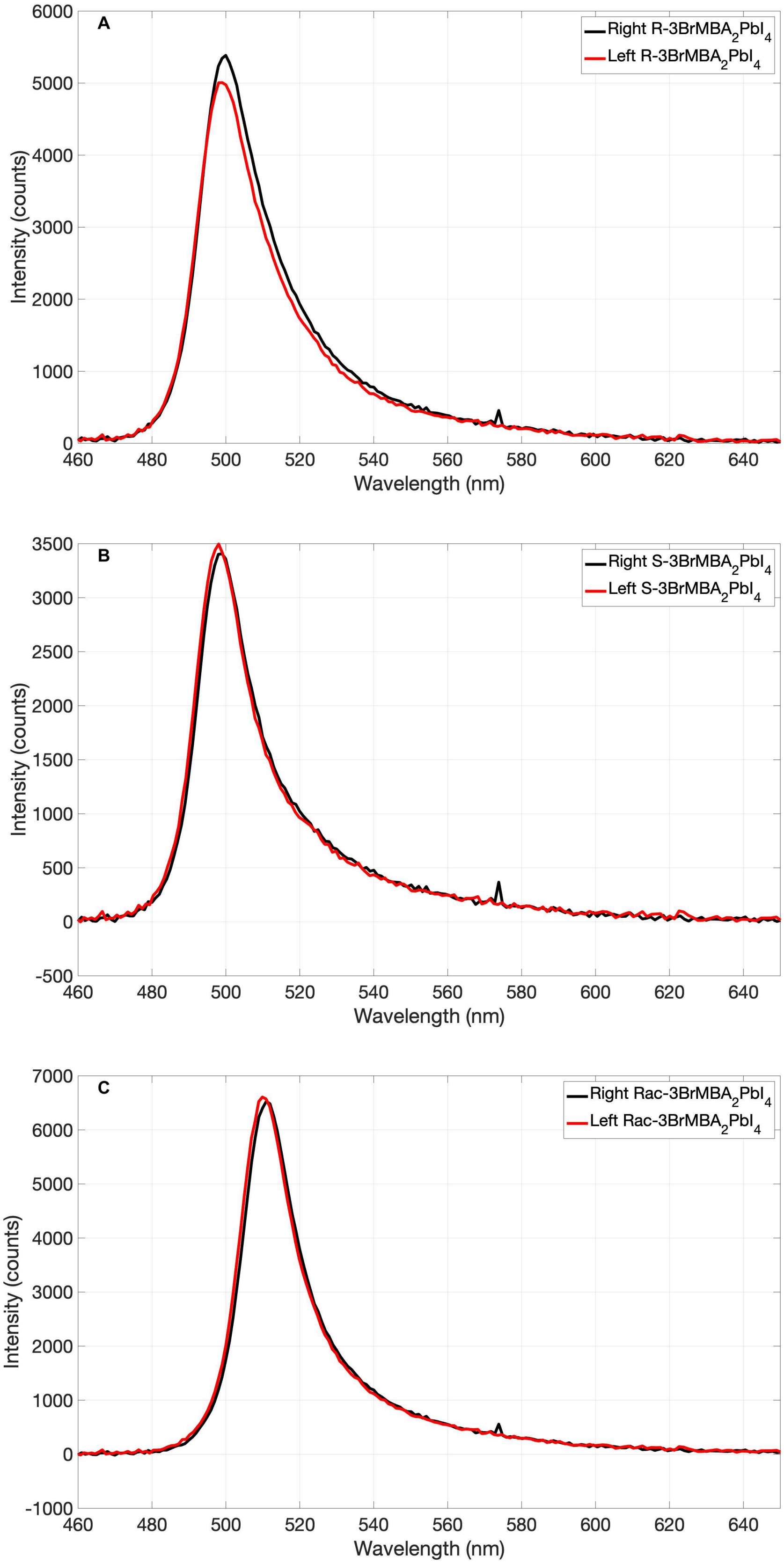

Figure S17. Measured right- and left-handed CPL of the spin-coated (A) *R*-3BrMBA$_2$PbI$_4$, (B) *S*-3BrMBA$_2$PbI$_4$, and (C) *Rac*-3BrMBA$_2$PbI$_4$ thin films via the space and time separated method under 450 nm excitation.

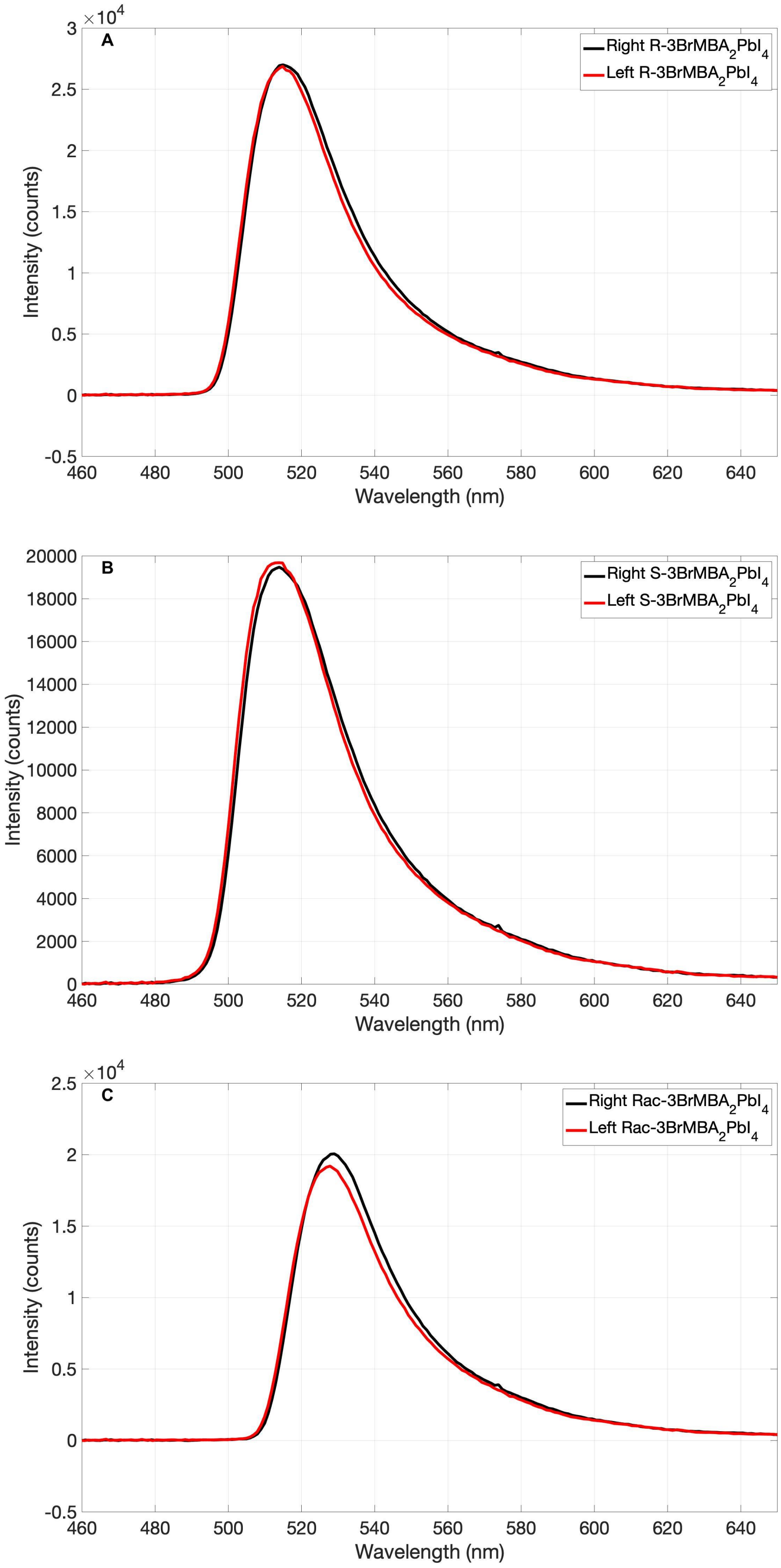

Figure S18. Measured right- and left-handed CPL of the drop-casted (A) *R*-3BrMBA$_2$PbI$_4$, (B) *S*-3BrMBA$_2$PbI$_4$, and (C) *Rac*-3BrMBA$_2$PbI$_4$ thin films via the space and time separated method under 450 nm excitation.

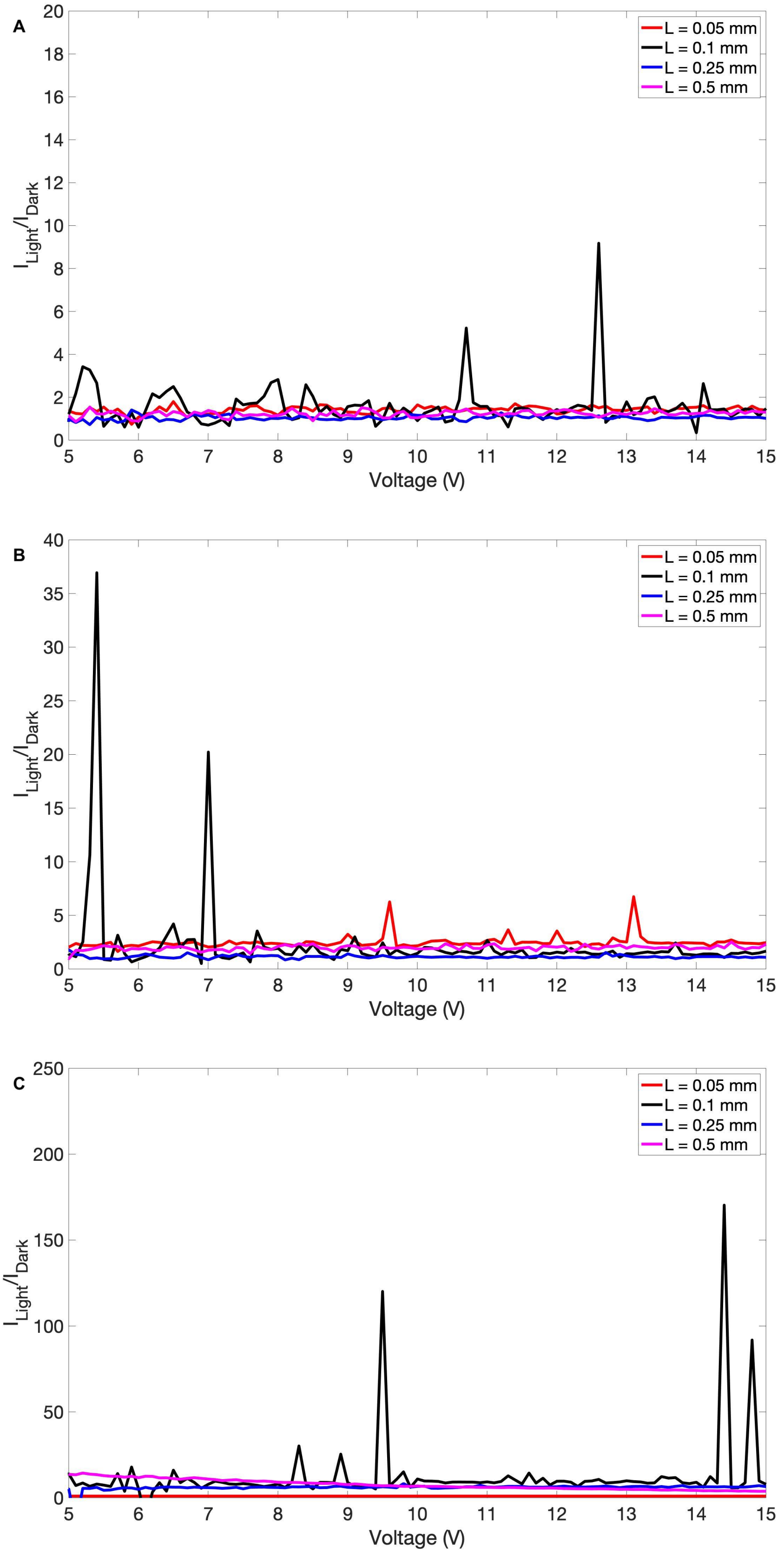

Figure S19. Calculated light/dark current ratio in function of voltage bias of the respective (A) *R*-MBA$_2$PbI$_4$, (B) *S*-MBA$_2$PbI$_4$, and (C) *Rac*-MBA$_2$PbI$_4$ thin films with varying electrode distances.

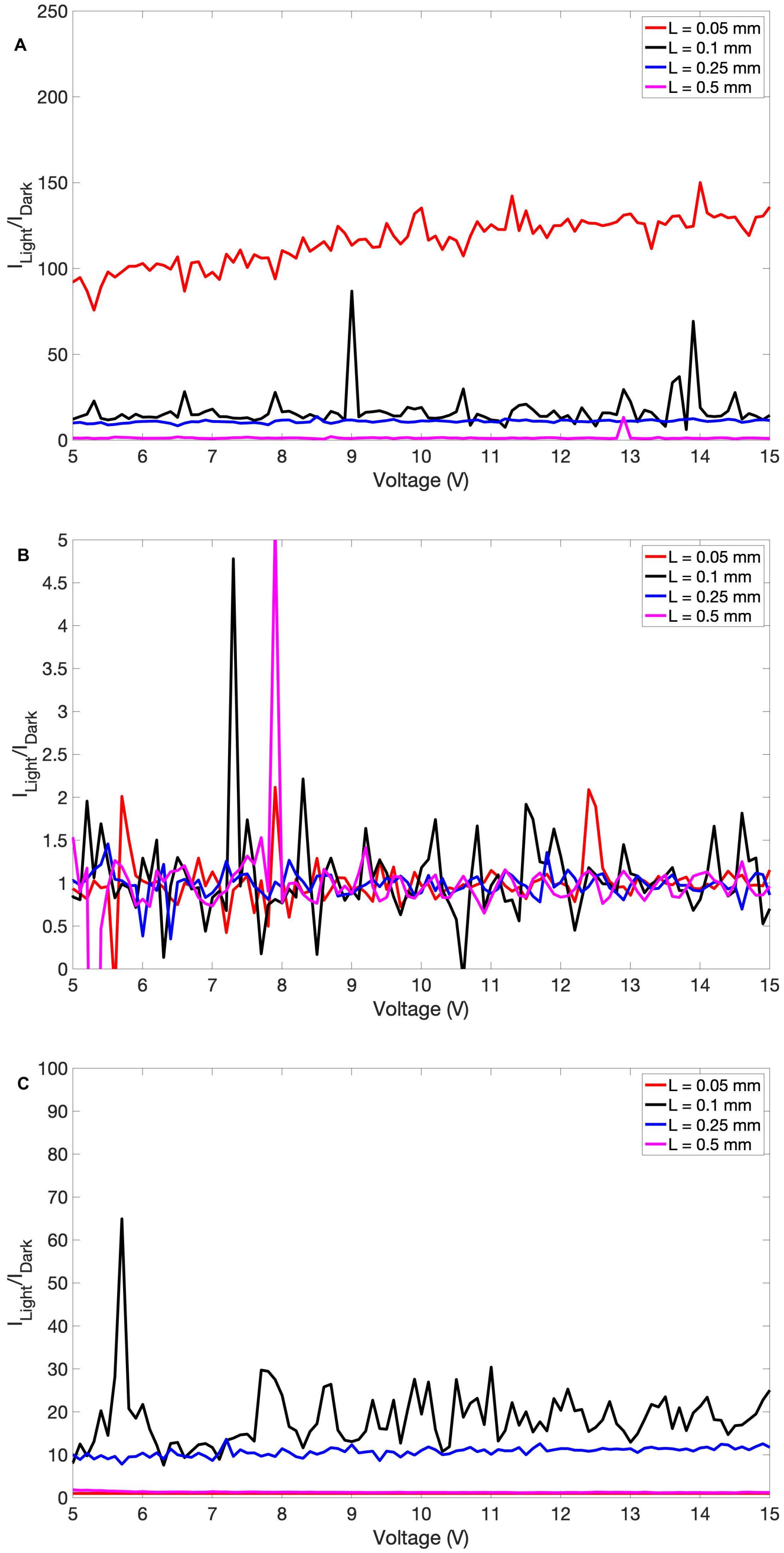

Figure S20. Calculated light/dark current ratio in function of voltage bias of the respective (A) *R*-3BrMBA$_2$PbI$_4$, (B) *S*-3BrMBA$_2$PbI$_4$, and (C) *Rac*-3BrMBA$_2$PbI$_4$ thin films with varying electrode distances.

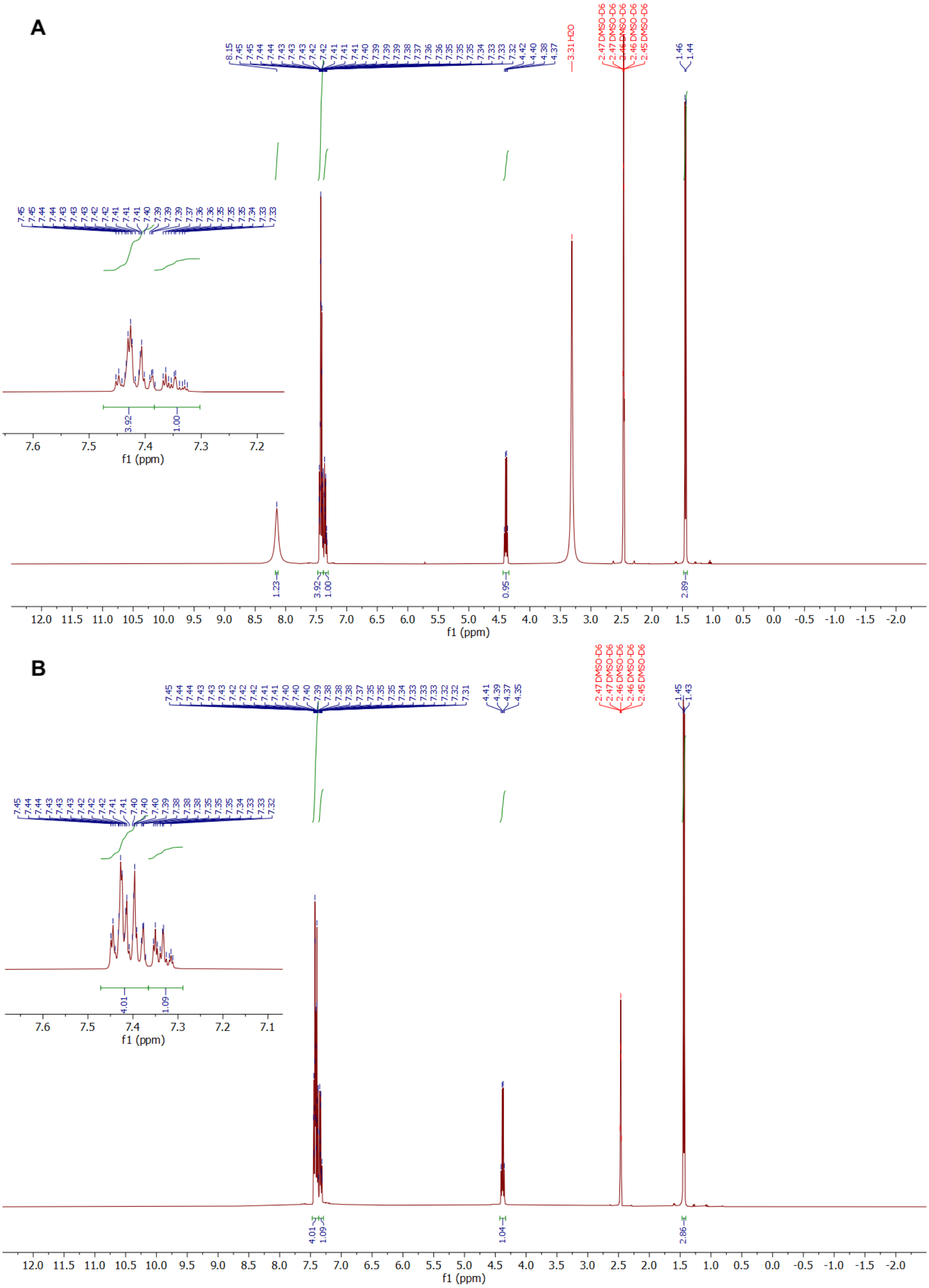

Figure S21. ^{1}H NMR spectra of (A) *R*-MBAI and (B) *S*-MBAI in DMSO-d6 (signal at 2.5 ppm). The signal at 3.33 ppm corresponds to residual water.

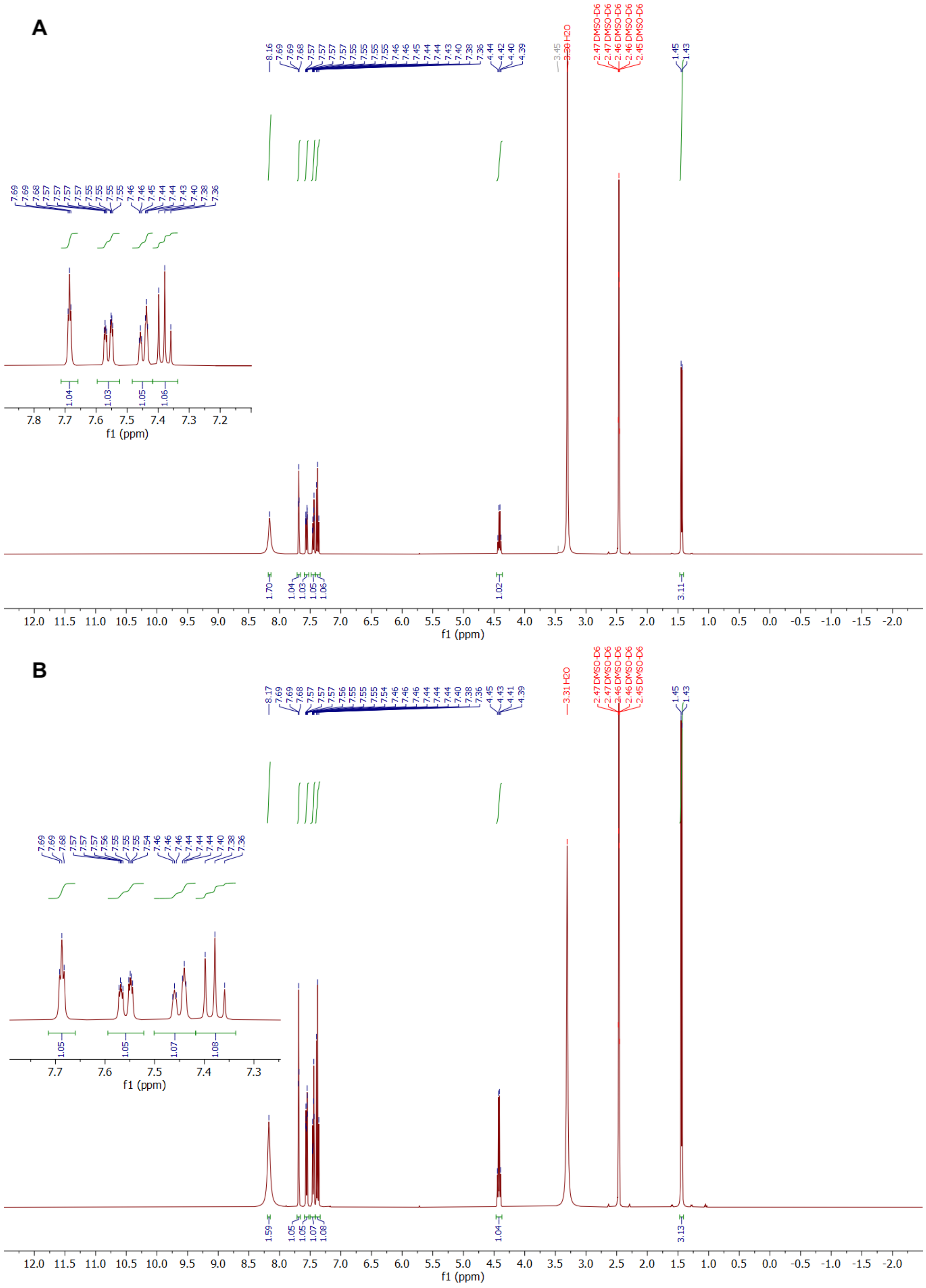

Figure S22. ^{1}H NMR spectra of (A) *R*-3BrMBAI and (B) *S*-3BrMBAI in DMSO-d6 (signal at 2.5 ppm). The signal at 3.33 ppm corresponds to residual water.

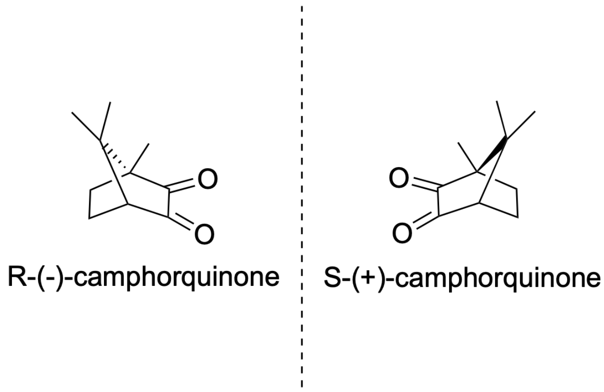

R-(-)-camphorquinone S-(+)-camphorquinone

Figure S23. Chemical structure of *R*-(-)-camphorquinone and *S*-(+)-camphorquinone.